

Structural and energetic heterogeneity in protein folding

Steven S. Plotkin and José N. Onuchic
Department of Physics, University of California, San Diego

A general theoretical framework is developed using free energy functional methods to understand the effects of heterogeneity in the folding of a well-designed protein. Native energetic heterogeneity arising from non-uniformity in native stability, as well as entropic heterogeneity intrinsic to the topology of the native structure are both investigated as to their impact on the folding free energy landscape and resulting folding mechanism. Given a minimally frustrated protein, both structural and energetic heterogeneity lower the thermodynamic barrier to folding, and designing in sufficient heterogeneity can eliminate the barrier at the folding transition temperature. Sequences with different distributions of stability throughout the protein and correspondingly different folding mechanisms may still be good folders to the same structure. This theoretical framework allows for a systematic study of the coupled effects of energetics and topology in protein folding, and provides interpretations and predictions for future experiments which may investigate these effects.

1. INTRODUCTION

Theories of protein folding currently focus primarily on predicting properties of the folding mechanism given the native structure and/or energy function is known *a priori*. The most powerful approach to this end has been the energy landscape theory, used in one form or another in most descriptions of folding [1–15]. This approach takes advantage of the huge number of conformational states available to a protein by treating the energetics of those conformations statistically, just as the description of a phase transition from a liquid to a crystal is understood through the application of statistical mechanics to the numerous degrees of freedom in the problem. However in understanding the self-organization of proteins and biological systems in general, it is necessary to study properties particular to finite-sized systems, e.g. barrier heights and corresponding rates. For a finite system such as a protein, characteristic features present in the amino acid sequence give rise to residual signatures in thermodynamic and kinetic properties. For example, although the four-helix proteins Im7 and Im9 are structural homologs, Im9 folds by a two-state mechanism while Im7 folds through an *en route* intermediate [16]: the free energy landscape may fluctuate sequence to sequence for aa chains that fold to the same native structure. Other experiments also indicate that rates and/or intermediates may differ for structural homologs [17, 18].

Since a knowledge of the native structure does not completely determine the free energy profile, we might ask what information does, and also what parameters must be known to predict other properties of the folding mechanism, such as the specificity or diffusivity of the folding nucleus, for example [19–22]. By analyzing the energetic statistics of ensembles of states, landscape theory provides a framework to distinguish folding processes common to an ensemble of sequences from those peculiar to individual sequences. A particular property, for example folding transition temperature T_F , is not strongly dependent on the detailed Hamiltonian of the protein, but only on a few thermodynamic parameters such as overall native stability, chain stiffness, overall variance in energies (if for example the sequence were thread through random structures), and perhaps also on chain length and overall hydrophobicity which induces generic collapse. The folding temperature may be expected to be a universal or self-averaging property for the ensemble of sequences having these parameters. Such quantities are important since they are amenable to analysis: the transition temperature may be expressed quantifiably through the parameters mentioned above as

$$T_F = \frac{z|\bar{\epsilon}|}{2s_o} \left(1 + \sqrt{1 - \frac{2s_ob^2}{z\bar{\epsilon}^2}} \right) \quad (1.1)$$

where $\bar{\epsilon}$ is the average native stability per residue ($\bar{\epsilon} < 0$), s_o is the entropy gain per residue in unfolding which depends on chain stiffness and also net hydrophobicity, b is the non-native energetic variance per residue, and z is the average number of neighbors per residue which is weakly a function of the chain length N . Equation (1.1) further gives the folding temperature for new sequences if these parameters can be determined, or conversely eq. (1.1) may help to determine intrinsic protein parameters from a measurement of the transition temperature. Equations for self-averaging properties provide a simple framework for understanding the phenomena; for

example if the variance is weak compared to the stability (the protein is well-designed) then the folding temperature is to the first approximation proportional to the stability gap over the entropy of unfolding: $T_F \approx -E_N/S_o$. So for example a well-designed stiff protein has a higher transition temperature than a flexible one, since it has less conformations per residue in the unfolded state. Moreover, by eq. (1.1) T_F is always below $z|\bar{\epsilon}|/s_o$ when non-native strength $b = 0$, so non-native interactions always lower the folding temperature by stabilizing the unfolded state. As b is increases, T_F decreases but remains real so long as [23]

$$\sqrt{\frac{z}{2s_o} \frac{|\bar{\epsilon}|}{b}} \geq 1, \quad (1.2)$$

the equality in (1.2) holding when T_F reaches its minimum value of $\sqrt{z/2s_o} b$ which is precisely the glass temperature T_G , defined as the temperature where the entropy of a random aa sequence is no longer extensive, i.e. where a random system becomes trapped in one of a small number of low energy states. Because T_F is found by equating the total free energy of the folded and unfolded states, it should be only weakly sensitive to the details of the actual distribution of native stability within the protein. On the other hand, properties such as the folding barrier and its corresponding rate may depend strongly on the distribution of native stability throughout the protein.

To theoretically treat the thermodynamics of folding and unfolding, we quantify a model protein in terms of the full native Hamiltonian $\{\epsilon_i\}$, as well as the full distribution of native contact lengths $\{\ell_i\}$, under the assumption that the protein under consideration is well-designed with T_F reasonably larger than T_G , i.e. the inequality (1.2) is easily satisfied. Native heterogeneity is retained explicitly, while non-native interactions are treated through an average background field- the scalar quantity b in eq.s (1.1) and (1.2). We are thus isolating the effects of native heterogeneity on the folding mechanism.

Certainly if the entropy around the transition state were small, as when the inequality (1.2) is not well-satisfied, the position and height of the rate determining barrier(s) would fluctuate wildly sequence to sequence. However, since proteins have evolved native stabilities larger than their RMS non-native energy scale [23–29] as manifested in inequality (1.2), the temperature T_F where the native state is stable is sufficiently higher than T_G , such that there is an extensive amount of residual entropy left under folding conditions. Nevertheless, we find that even though there is a large entropy present in the system, there are still in fact strong dependencies of the barrier and folding mechanism on the distribution of native stability and distribution of native contact lengths. In fact local fluctuations in native stability and structure do not average out, but contribute extensively in determining properties of the folding mechanism!

For a property which is not self-averaging over a given ensemble of sequences, the parameters specified to determine the ensemble are either not sufficiently accurate or are incomplete. For example, the folding transition temperature T_F is not self-averaging over the ensemble of sequences that fold to a particular native structure, since these different sequences may have different native stability, flexibility, etc. Nonetheless, a quantity such as folding temperature or folding barrier which fluctuates over an incompletely specified ensemble may have a mean that is still useful in characterizing trends as a function of one or more parameters. An example is the increase on average in folding rate, or decrease in folding barrier, as mean native contact length $\bar{\ell}$ (more specifically $\bar{\ell}/N$) is decreased [30], for which several models have been proposed [31, 32], and which we consider here within our theoretical framework as well (see section 5.5.G). The observed correlation between rates and $\bar{\ell}$ implies that many proteins are sufficiently well-designed such that native topology plays an important if not dominant role in governing folding mechanism, a topic recently investigated by several authors [31–42].

Our intention here is to go beyond the first moment of the contact length distribution $\bar{\ell}$ or stability distribution $\bar{\epsilon}$. We investigate how the full distributions of energetics and topology as well as correlations between them affects the free energy profile, corresponding barrier, folding rate, and overall folding mechanism. For one example, we find in section 5.5.H that there is a net correlation between structural variance defined through the second moment of the contact length distribution and folding rate for well-designed proteins with a given mean contact length $\bar{\ell}$. Expanding on our previous work [43], we find that native heterogeneity, both entropic and energetic, plays an important role in quantifying protein folding mechanisms. We show how one can extend the analysis of thermodynamic quantities by using functionals to describe folding properties which are not necessarily self-averaging but which may depend on distributions of coupling parameters. To this end we derive a simple field theory with a nonuniform order parameter to study fluctuations away from uniform ordering, through free energy functional methods introduced earlier by Wolynes and collaborators [34, 44, 45]. The theory is in good agreement with lattice simulations also performed in this paper. Similar effects have also been observed in Monte Carlo simulations of sequence evolution for lattice protein models, when the selection criteria involves fast folding rate [46]. Here we see how, from general considerations of the energy landscape

theory, selecting for rate can induce heterogeneity in the transition state ensemble. The folding barrier for a well-designed protein is maximized when the nucleus is the most diffuse. For typical values of native energies, well-designed proteins have heterogeneous funneled folding mechanisms [47–51].

Our results are also supported by several experiments in the literature as described in the conclusions section, and suggest experiments to be performed. For example the reduction of barrier height with folding heterogeneity should be experimentally testable by measuring the dependence of folding rate for a well-designed protein on the dispersion of ϕ -values [52]. It is important that before and after the mutation(s) the protein remains fast-folding to the native structure without “off-pathway” intermediates, and that its native state stability remain approximately the same, perhaps by tuning environmental variables.

In the arguments below we associate reductions in the free energy barrier ΔF^\ddagger to increases in the folding rate k_F . This is true as long as the prefactor k_o in the expression for the rate

$$k_F = k_o e^{-\Delta F^\ddagger/T} \quad (1.3)$$

is more weakly affected than the barrier height under redistribution of native stability. While the distribution of native stability must indeed couple with the specific distribution of non-native interactions, for well-designed proteins with large transition-state entropy, it is more likely that the effect on the prefactor comes from the coupling of the transition temperature T_F to the distribution of native stability, as long as the protein still folds to the same native structure. In other words we must consider the effect on the prefactor as the ratio of the transition temperature to glass temperature T_F/T_G changes, i.e. as the left hand side of (1.2) changes and the protein becomes more or less well-designed. However we find (see fig.s 12 and 19) that even for perturbations in native energy large enough to kill the barrier, the folding temperature varies only weakly compared to the changes in barrier height, so that the ratio T_F/T_G should also not vary significantly compared to the changes in barrier height. Thus the barrier height is the strongest determinant of folding rate in well-designed proteins. For Gō-like models with native interactions alone, the energy distribution does not strongly affect the prefactor: rates obtained from simulations are well fit with those predicted from the change in barrier height alone (see fig. 18), i.e. the energy distribution does not strongly affect the reconfiguration kinetics appearing in the prefactor, compared to its effect on the barrier height. For a full discussion of the above effects see section 5.5.F.

When the Hamiltonians consists of pair interactions alone, redistributions of native stability can eliminate the barrier entirely at the folding temperature, see figures 11 and 17. It is worth noting that many-body interactions which are believed to be present in real protein interactions [53–59] tend to increase the barrier height [60–62], and in their presence the barrier may be more robust to redispersment of native stability.

A funnel folding mechanism consisting of a large number of routes to the native structure is preserved for a wide variety of folding scenarios and barrier heights, including folding through on-pathway intermediates. For the distributions of native energy necessary to induce folding through one or a few routes, the folding temperature drops by about a factor of six, which indicates that for realistic energy functions which are also composed of non-native interactions, folding would be exceedingly slow at the low temperatures where the native state would be stable. However for proteins which are large and multi-domain, it is possible that entropic or energetic heterogeneity may induce significantly route-like folding near the transition temperature.

The paper is organized as follows. First in section 2 we outline the strategy of the calculation and illustrate it with a simple example in section 2.2.A. Next we anticipate and explain several of the results with physical arguments in section 3; its reading is not essential for the rest of the paper, but should be very helpful to the reader. In section 4 the full expression for the free energy functional is derived, and the functional is implemented in section 5 where comparison is made to the results from lattice simulations. Finally we conclude and suggest future research.

2. THE GENERAL STRATEGY

It is first necessary to characterize the generic properties of the native state. We adopt a coarse grained description for the native structure, and describe it by its distributions of native contact energies $\{\epsilon_i\}$ and native loop lengths or contact lengths $\{\ell_i\}$ (see figure 1). Here ϵ_i is the solvent averaged effective energy of contact i , and ℓ_i is the sequence length pinched off by contact i (see fig. 1) [63]. We use a single subscript for the labeling index i because we are only considering effects on the particular set of native contacts for a given native structure. Non-native interactions are treated by an average field, since the protein is assumed to be well-designed to its native structure, and native interactions are then most important in determining the folding mechanism. The index i runs from 1 to M , where M is the number of residue pair contacts in the

lowest energy native structure. M scales roughly extensively, i.e. $M = zN$, with N the number of residues in the polymer chain. Here z is the mean number of contacts per residue: a function of either the lattice coordination number or the off-lattice cut-off length. It is of order 1, with surface area corrections dying away as $N^{-1/3}$ [64]. We can quantify nativeness in the first approximation by the fraction of native contacts Q , with $0 < Q < 1$. Other parameters are also reasonable for stratifying the landscape: the fraction of correct (native) dihedral angles [27], coarse grained position in space in the native structure [65,66], or even the ensembles having a given probability to fold before unfolding [67]. But Q is the most suitable for calculation in the present theory. At partial degrees of nativeness the probability to form contact i is defined as $Q_i(Q)$, and we define $Q_i^*(Q)$ as the fraction of time contact i is formed at equilibrium in the ensemble with MQ native contacts, or equivalently the fraction of proteins in a macroscopic sample with a given degree of nativeness having that contact formed. Non-uniformity in Q_i^* values at partial degrees of nativeness would indicate that the protein prefers to fold some regions over others.

Following the formalism used in inhomogeneous fluids [68,69] and the theory of first order transitions [70] we write a free energy functional $F(\{Q_i\}, \{\epsilon_i\}, \{\ell_i\})$ to characterize the effects of structural and energetic heterogeneity superimposed on the overall folding funnel. This approach has been used earlier by Bohr and Wolynes to describe domain growth in proteins [71] and more recently as a calculational tool for experimental ϕ -values [34, 44, 45].

The free energy functional is first interpreted as depending upon the local contact probabilities $Q_i(Q) = \langle \Theta(r_i - r_i^N) \rangle_T(Q)$ where i labels the native contact between two residues, r_i the distance between them, Θ is a function that measures proximity such as a step function for off-lattice models or a Kronecker delta for non-bonded nearest neighbor sites on-lattice, and $\langle \dots \rangle_T$ indicates the an average over the ensemble at Q . We will typically take $\langle \dots \rangle_T$ to be a Boltzmann weighted average; then Q_i^* is the thermally averaged fraction of the time two parts of the protein are in proximity (contact) [72]:

$$Q_i^*(Q) = \langle \delta_i \rangle_T = \sum_{c \in Q} \delta(i, c) \frac{\exp(-E_c/T)}{Z} \quad (2.1)$$

where $\delta(i, c) = 1$ if contact i is made in configuration c , and $\delta(i, c) = 0$ otherwise. The sum may be taken over any ensemble of theoretical interest. Here we have in mind the ensemble defined as having a given degree of overall order $Q = (1/M) \sum_i Q_i$ [73].

In the functional method, all the contact energies $\{\epsilon_i\}$ and loop lengths $\{\ell_i\}$ for a protein are initially assumed as given, and the thermal (most probable) distribution of contact probabilities $\{Q_i^*(\{\epsilon_i\}, \{\ell_i\}, Q)\}$ is found by minimizing the free energy functional $F(\{Q_i(Q)\} | \{\epsilon_i\}, \{\ell_i\})$ with respect to the distribution of occupation probabilities, subject to the constraint that the average probability is Q , i.e. $\sum_i Q_i = MQ$ (Q then parameterizes the values of the Q_i^* s). Examples of the functions $Q_i^*(Q)$ are plotted in figures 2 and 14. This procedure is analogous to finding the most probable distribution of occupation numbers, and thus the thermodynamics, by maximizing the microcanonical entropy for a system of particles obeying a given occupation statistics. Here the effective particles (the contacts) obey Fermi-Dirac statistics, (see eq. (4.35)), since no more than one bond can “occupy” a contact. The system can be understood to have a set of free energy levels obeying a distribution governed by the native structure and energies of the protein, and we seek the fraction of time (the probability) those levels are occupied given a fixed overall number of levels filled.

The free energy for a system obeying the thermal (most probable) distribution $\{Q_i^*(Q, \{\epsilon_i\}, \{\ell_i\})\}$ is then considered a function of the contact energies for a *fixed* native structure: $F(Q, \{\epsilon_i\} | \{\ell_i\})$. That is, we consider the folding free energy barrier as a functional of the interaction energies $\{\epsilon_i\}$ for a *given* native topology. The free energy depends on the energies $\{\epsilon_i\}$ both explicitly and implicitly through the thermal contact probabilities $\{Q_i^*(\{\epsilon_i\} | Q, \{\ell_i\})\}$. Then we can seek the special distribution of contact energies $\{\epsilon_i^*(\ell_i)\}$ that extremizes (minimizes or maximizes, depending on the second derivative) the thermodynamic folding barrier to a particular structure by finding the extremum of $F^\dagger(\{\epsilon_i\} | \{\ell_i\})$ with respect to the contact energies ϵ_i , subject to the constraint of fixed total native energy: $\sum_i \epsilon_i = M\bar{\epsilon} = E_N$, i.e. while maintaining the same overall stability of the native structure. Thus we are isolating the effect of heterogeneity on the folding mechanism. This distribution when substituted into the free energy gives in principle the extremum free energy barrier as a function of native structure $F^\dagger(\{\ell_i\})$, which might then be optimized for the fastest/slowest folding structure and its corresponding barrier. However we found that in fact the only distribution of energies for which the free energy was an extremum is in fact the distribution which *maximizes* the barrier by tuning all the contact probabilities to the same value: $Q_i(Q^\dagger) = Q^\dagger$. In this case the coupling energies would be tuned to eliminate any information contained in the native structure, except for the mean loop length $\bar{\ell} = (1/M) \sum_i \ell_i$. Any perturbation away from this scenario lowers the free energy barrier. We also examine

the effects of structural dispersion on the barrier, i.e. a free energy for variable loop distribution but fixed coupling energies $F(Q, \{\ell_i\} | \{\epsilon_i\})$, and arrive at the same conclusion: for fixed energies, increasing structural variance (at fixed average loop length) lowers the barrier and thus speeds the rate, as long as the protein is sufficiently well-designed that the rate is governed by the free energy barrier.

2.A. An example

We illustrate the procedure by applying it to a more trivial system- an Ising paramagnet in a non-uniform external field. The Hamiltonian for this system is

$$\mathcal{H} = - \sum_{i=1}^N \epsilon_i \sigma_i, \quad (2.2)$$

where $\sigma_i = \pm 1$ is the i th spin and ϵ_i is its local field energy. To obtain the free energy functional we need an expression for the entropy in terms of the spin degrees of freedom. If the field was uniform, the entropy per spin $s(q)$ could be written in terms the fraction of up spins $N_+/N \equiv q$ as

$$s(q) = \frac{S(q)}{N} = \frac{1}{N} \ln \frac{N!}{(Nq)! [N(1-q)]!} \cong [-q \ln q - (1-q) \ln(1-q)]. \quad (2.3)$$

Here $q = (1 + \bar{\sigma})/2$ where $\bar{\sigma} = (1/N) \sum_i \sigma_i$ is the average magnetization per site. However if the field varies from site to site so will the equilibrium value of the spin. To allow for this the entropy per spin must be written in terms of $q_i = (1 + \sigma_i)/2$, and the total entropy is then a functional $S(\{q_i\})$. The free energy functional is then

$$F(\{\sigma_i\}, \{\epsilon_i\}) = \sum_{i=1}^N \left[-\epsilon_i \sigma_i + T \left(\frac{1 + \sigma_i}{2} \ln \frac{1 + \sigma_i}{2} + \frac{1 - \sigma_i}{2} \ln \frac{1 - \sigma_i}{2} \right) \right]. \quad (2.4)$$

The equilibrium values of the spins σ_i^* are obtained by finding the extremum of the free energy, perhaps subject to a fixed overall magnetization [74] $M = \sum_i \sigma_i$:

$$\frac{\delta}{\delta \sigma_i} \left(F + h_M \sum_j \sigma_j \right) = 0. \quad (2.5)$$

This leads to the equation

$$\sigma_i^* = \tanh \left(\frac{\epsilon_i + h_M}{T} \right) \quad (2.6)$$

for the equilibrium values of the spins. Each spin follows its local field according to the well-known Brillion function (for spin 1/2). The Lagrange multiplier h_M is determined from the sum $\sum_i \sigma_i^* = M$. For a uniform field ϵ , $h_M = T \tanh^{-1}(M/N) - \epsilon$. The second variation of F is positive indicating the free energy is minimized and σ_i^* are the thermal equilibrium values:

$$\left. \frac{\delta^2 F}{\delta \sigma_i \delta \sigma_j} \right|_{\{\sigma_i^*\}} = \delta_{ij} \frac{T}{1 - \sigma_i^{*2}} > 0. \quad (2.7)$$

Substituting $\sigma_i^*(\epsilon_i)$ (eq. (2.6)) back into the free energy functional (2.4) gives the free energy in terms of the coupling energies $\{\epsilon_i\}$:

$$\frac{F(\{\epsilon_i\})}{T} = -N \ln 2 - \sum_{i=1}^N \ln \left[\cosh \left(\frac{\epsilon_i + h_M}{T} \right) \right] + \frac{h_M M}{T}. \quad (2.8)$$

This is equivalent to the form obtained from the partition function in the canonical ensemble.

Now we can seek the set of fields ϵ_i^* that extremizes the free energy subject to a given total coupling energy $E = \sum_i \epsilon_i$:

$$\frac{\delta}{\delta\epsilon_i} \left(F + p \sum_j \epsilon_j \right) = 0. \quad (2.9)$$

This yields the condition that all the spins have the same value and thus that the field be uniform:

$$\sigma_i(\epsilon_i^*) = p \quad (2.10)$$

$$\epsilon_i^* = \epsilon \quad (2.11)$$

However, second variation of the free energy gives

$$\left. \frac{\delta^2 F}{\delta\epsilon_j \delta\epsilon_i} \right|_{\{\epsilon_i\}=\{\epsilon\}} = -\delta_{ij} \frac{1}{T} \operatorname{sech}^2 \left(\frac{\epsilon + h_M}{T} \right) \quad (2.12)$$

which is negative, indicating this choice of coupling energies *maximizes* the free energy. Thus any perturbations away from the uniform field will lower the free energy. Although the entropy functional is much more complicated for proteins, we find that there too the only free energy extremum is a maximum.

3. PHYSICAL ARGUMENTS FOR THE EFFECTS

Before we present the full free energy functional theory, we include here some physically motivated arguments for the effects to give the reader a deeper intuitive feel for the results derived later within the more general framework. This section is fairly independent of the rest of the text; it is broken up into subsections which may be skipped or read in any order. The first subsection concerns the effect on rates by changing the interaction energies of contacts that are likely or unlikely to begin with. The second subsection consists of various proofs describing how heterogeneity lowers the barrier and the consequences of this phenomenon, and in the third subsection we show a simple proof that a protein with stability distributed uniformly has maximal conformational entropy.

3.A. Making early-forming native contacts relatively stronger will tend to speed folding more than making late-forming native contacts relatively stronger by the same amount

The argument proceeds as follows [75]. First notice that

$$\frac{\partial F}{\partial\epsilon_i} = \frac{\partial}{\partial\epsilon_i} (-T \ln Z) = \frac{1}{Z} \sum_c \frac{\partial E_c}{\partial\epsilon_i} e^{-E_c/T}, \quad (3.1)$$

where the sum is over all the states with a given similarity Q to the native. Since the energy of conformation c is a sum of its contact energies: $E_c = \sum_{j \in c} \epsilon_j$, $\partial E_c / \partial\epsilon_i = \delta(i, c)$ and thus by eq. (2.1)

$$\frac{\partial F}{\partial\epsilon_i} = Q_i. \quad (3.2)$$

This result, derived below within the functional formalism (c.f. eq. (5.8)), means that the change in free energy δF in perturbing a contact i an amount $\delta\epsilon_i$ is equal to the amount of that perturbation times the fraction of time that contact is formed. An analogous equation holds for an inhomogeneous fluid, where the density of fluid at position \mathbf{x} , $n(\mathbf{x})$, plays the role of contact probability and the external field at \mathbf{x} , $u(\mathbf{x})$, plays the role of the perturbation: $\delta F / \delta u(\mathbf{x}) = n(\mathbf{x})$.

Now imagine taking two contacts $i = 1, 2$ within the protein having formation probabilities Q_1, Q_2 , and making equal and opposite energetic perturbations on them $\delta\epsilon > 0$ (see fig. 3). Now by eq. (3.2), the total change in free energy to first order is

$$\delta F \cong -Q_1 \delta\epsilon + Q_2 \delta\epsilon = -(Q_1 - Q_2) \delta\epsilon \quad (3.3)$$

so if $Q_1 > Q_2$ the change in free energy is negative and if $Q_2 > Q_1$, $\delta F > 0$. Since contacts are *typically* unformed or less formed in the unfolded state, we can say that if $Q_1(Q^\dagger) > Q_2(Q^\dagger)$, $\delta\Delta F^\ddagger < 0$ and *vice-versa*. Since for well-designed two-state folders the rate is controlled by the free energy barrier, the assertion

is then demonstrated (c.f. the discussion in the introduction regarding barrier governed rates, and also see section 5.5.F). Some obvious caveats include perturbations on a protein not well-designed, perturbations of contacts involving residues anomalously formed in the unfolded state, or situations where strengthening one of the contacts lowers the free energy of an on-pathway intermediate; for these exceptional cases the effect may not be observed.

3.B. Adding native heterogeneity will always lower the thermodynamic folding barrier in a well-designed protein.

A homogeneously ordering protein is equally likely to fold from anywhere within it. As perturbations are made away from this scenario, say in native interaction energies or through structural variance, the folding barrier tends to decrease. Several arguments detailed in the following subsections suggest this effect.

3.B.1. Random Energy Model method

Consider making random energetic perturbations on the contact energies of an initially homogeneous idealized system (where all contact probabilities are the same: $Q_i = Q$) with free energy barrier F_{HOMO} and folding rate $k_o \exp(-F_{\text{HOMO}}/T)$. Then the new rate is

$$k_f = k_o \exp\left(-\frac{F_{\text{HOMO}} + \delta F(T)}{T}\right) = k_{\text{HOMO}} \exp\left(-\frac{\delta F(T)}{T}\right). \quad (3.4)$$

If the total native (unconstrained) energetic variance $\sum_i \delta \epsilon_i^2$ is ΔE_N^2 , the variance at the transition state is approximately $\Delta E_N^{2\dagger} = Q^\dagger(1 - Q^\dagger)\Delta E_N^2$, given the energies must sum to total native energy E_N . The variance vanishes at $Q = 0$ since there are no contacts made there, and vanishes at $Q = 1$ since all the $\sum_i \epsilon_i = E_N$, i.e. all the energies must sum to a fixed number and thus their sum cannot vary. Approximating the transition state as an ensemble of states with uncorrelated energies, i.e. a random energy model [76], and considering only the effects of changing native interactions, the energy will always decrease twice as much as the entropy times the temperature under the influence of heterogeneity. Thus the free energy barrier decreases:

$$\delta F(T) = \delta E(T) - T\delta S(T) = -\frac{\Delta E_N^{2\dagger}}{T} - \frac{\Delta E_N^{2\dagger}}{2T} = -\frac{Q^\dagger(1 - Q^\dagger)\Delta E_N^2}{2T}, \quad (3.5)$$

and the rate in eq. (3.4) increases as

$$k_f \approx k_{\text{HOMO}} \exp\left(\frac{Q^\dagger(1 - Q^\dagger)\Delta E_N^2}{2T^2}\right). \quad (3.6)$$

This crude argument yields essentially the same result as a much more detailed functional analysis, c.f. eq. (5.19) of the text; an additional factor appears there to account for polymer effects on the number of routes to the native state. By this argument even for an initial unperturbed funnel which is fully symmetric (an idealized case where all contacts are equally likely to be formed), introducing arbitrary heterogeneity lowers the folding barrier.

As we will see below, since energies and entropies enter the expression for Q_i on the same footing, the above statements apply to the dispersion in loop entropies inherent to a particular native structure, see fig. 22.

3.B.2. Argument from Transition state theory

The result (3.6) is not surprising from the point of view of transition state theory. Another way of describing it is to note that the time rate of change of the population \mathcal{N} in a metastable state is proportional to the escape rate, and the escape rate is itself proportional to the ratio of partition functions, transition state to reactant:

$$\frac{\dot{\mathcal{N}}}{\mathcal{N}} = k \sim \frac{Z^\ddagger}{Z^o}. \quad (3.7)$$

Now we imagine the transition state to be composed of an ensemble of Ω^\ddagger microstates of the system having energies $E_i^\ddagger = \bar{E}^\ddagger + \delta E_i$, where δE_i is distributed state to state from a Gaussian distribution: $P(\delta E_i) \sim \exp(-(\delta E_i)^2/2Nb^2)$. Then

$$Z^\ddagger = \sum_i e^{-\beta E_i^\ddagger} \sim e^{-\beta \bar{E}^\ddagger} \Omega^\ddagger \langle e^{-\beta \delta E} \rangle = \bar{Z}^\ddagger e^{Nb^2/2T^2}. \quad (3.8)$$

So, neglecting changes in the prefactor, the rate increases exponentially with the variance in the transition state, which scales extensively with system size.

3.B.3. Optimum fluctuation method

Applications of nucleation in disordered media [77, 78] to protein folding show similar trends in the folding rate. In a system such as a protein there may be regions where nucleation of the folded state is favored due to local energetic or entropic inhomogeneities. These may speed the rate of nucleation by decreasing the effective thermodynamic nucleation barrier, referred to in the nucleation literature as the optimum fluctuation (see fig. 4). In the theory of electronic band tails in disordered systems the optimum fluctuation method has been used to calculate the density of states at the mobility edge [79–81].

Let the folding rate for a given nucleation barrier F^\ddagger be $k(F^\ddagger) = k_o \exp(-F^\ddagger/T)$ and the probability distribution of nucleation barriers be defined as $P(F^\ddagger) \equiv \exp(-\phi(F^\ddagger))$. Then the average rate in the presence of a distribution of barriers is

$$\bar{k} = \int dF P(F)k(F) \approx k_o e^{-G(T)} \quad (3.9)$$

where

$$G(T) = \min_F \left(\phi(F) + \frac{F}{T} \right) \quad (3.10)$$

The decrease in activation barrier by the REM argument above amounts to letting the free energy barriers be Gaussianly distributed about a mean \bar{F}^\ddagger with variance Δ^2 , so $\phi(F) \approx (F - \bar{F}^\ddagger)^2/2\Delta^2$. Then straightforwardly from (3.10) the effective barrier $F^*(T) = \bar{F}^\ddagger - \Delta^2/T$ and thus

$$\bar{k} \approx k_o \exp \left(-\frac{\bar{F}^\ddagger}{T} + \frac{\Delta^2}{2T^2} \right) = k_{\text{HOMO}} \exp \left(\frac{\Delta^2}{2T^2} \right), \quad (3.11)$$

which has the same form as eq. (3.6), since this is essentially the same argument as above.

We could have just as well found the disorder averaged time to nucleate a folded structure, from $\bar{\tau} = \int P(F)\tau(F) = \tau_o \exp(\bar{F}^\ddagger/T + \Delta^2/2T^2)$. Large barriers increase the mean time above zero-disorder value when the averaging is done. This does not mean the rate observed in an experiment slows, since the important quantity governing the decrease in reactant population is the transition rate k , as described above in section 3.3.B.3.B.2.

Example: Free energy potentials observed in simulations. Consider for example the free energy profile obtained from off-lattice Monte Carlo simulations of a uniform energy $G\bar{o}$ model to the native structure of CheY (see fig. 5). The profile is obtained by Boltzmann sampling the states and partitioning them to different ensembles given their overall number of native contacts. This profile is proportional to the function $G(T)$ above in eq. (3.10), i.e. it contains by construction the reduction in barrier due to structural (entropic) fluctuations, and so should be a good predictor of the rate. The probability a particular native core (illustrated in fig. 6) is sampled is

$$p_C \approx e^{-E_C/T+S_H} = e^{-F_C/T} \quad (3.12)$$

where E_C is the energy of the native core ($E_C = E_N Q$ for all cores in the uniform $G\bar{o}$ model) and S_H is the entropy of the polymer halo dressing the core. The role of native cores and halos in calculating free energy profiles was discussed in [61]. So up to a Q independent constant, the free energy at Q is obtained from the relative probabilities as

$$\begin{aligned}\frac{F}{T}(Q) &\sim -\log \left[\sum_{\text{CORES}}^Q e^{-F_C/T} \right] \\ &\sim -\log \int' dF_C n(F_C) e^{-F_C/T}\end{aligned}\quad (3.13)$$

where the sum has been replaced by an integral over the number of cores at Q having free energy F_C . Equation (3.13) is analogous to eq.s (3.9) and (3.10) above obtained from the optimum fluctuation method. As a limiting case consider an idealized folding funnel with no dispersion in energetics or entropics. Then $n(F_C) = \exp(S_{\text{ROUTE}})\delta(F_C - \bar{F}_C)$, where $\exp(S_{\text{ROUTE}})$ is the number of cores, or routes through the bottleneck. The free energy in (3.13) then becomes

$$\frac{F}{T}(Q) \sim \frac{E(Q)}{T} - \bar{S}_H(Q) - S_{\text{ROUTE}}(Q) \quad (3.14)$$

which reproduces the mean-field free energy profile [61] in the absence of non-native interactions. When there is dispersion in the free energies of a partially structured protein, there is a distribution of core free energies. Heuristically we can approximate this by a Gaussian distribution:

$$n(F_C) = e^{S_{\text{ROUTE}}} P(F_C) \approx \exp \left(S_{\text{ROUTE}} - \frac{(F_C - \bar{F}_C)^2}{2\Delta^2} \right). \quad (3.15)$$

Then

$$\begin{aligned}\frac{F}{T}(Q) &\sim -S_{\text{ROUTE}}(Q) - \log \left[\int' dF_C e^{-F_C/T - (F_C - \bar{F}_C)^2/2\Delta^2} \right] \\ &\sim -S_{\text{ROUTE}}(Q) + \frac{\bar{F}_C}{T} - \frac{\Delta^2}{2T^2}.\end{aligned}\quad (3.16)$$

So the barrier observed by sampling the Monte Carlo data or running molecular dynamics is the optimal fluctuation barrier, which includes in it the lowering effect due to structural dispersion in fig. (5) and both structural and energetic dispersion in general. The lowering of the barrier due to structural variance is further investigated in section 5.5.H (see also fig. 22). Additionally, experiments which monitor equilibrium properties related to relaxation rates or native structure formation measure the optimum fluctuation, as mentioned above in the context of transition state theory. $S_{\text{ROUTE}}(Q)$ in eq. (3.16) is the log of the total number of possible native cores at Q . This quantity will appear in the free energy functional below, where after the functional is minimized it is interpreted as the number of thermally accessible routes at a given temperature.

3.B.4. Thermodynamic perturbation theory

Another argument for the lowering of the barrier makes use of thermodynamic perturbation theory [82]. Consider a \bar{G}_0 model with M contacts, whose configurational states are perturbed in energy by a random contribution $V_c \equiv \delta E_c$ so that the new energy of state c is $E_c = E_c^0 + V_c$. Let the native energy be unchanged: $\delta E = 0$ in the native state. Then the change in free energy to second order in V is

$$\delta\Delta F(Q) = \langle V \rangle - \frac{1}{2T} \langle (V - \langle V \rangle)^2 \rangle \quad (3.17)$$

where

$$\langle V \rangle = \frac{1}{Z} \sum_{c \in Q} V_c \exp(-E_c^0/T) = \langle \delta E \rangle'_o \quad (3.18)$$

is calculated by summing over all configurations c having Q native contacts. Now since the change in a configuration's energy is the sum over perturbations of native contacts made in that state,

$$\begin{aligned}
\langle \delta E \rangle'_o &= \sum_{c \in Q} \delta E_c \frac{e^{-E_c/T}}{Z} \\
&= \sum_{c \in Q} \sum_{j \in c_N} \delta(j, c) \delta \epsilon_j \frac{e^{E_c/T}}{Z} = \sum_{j \in c_N} \langle \delta_j \delta \epsilon_j \rangle \\
&= \sum_{j=1}^M \langle \delta_j \rangle \delta \epsilon_j = \sum_{j=1}^M Q_j \delta \epsilon_j.
\end{aligned} \tag{3.19}$$

The last equality follows from eq. (2.1). Thus the first order change in free energy is simply the sum of the perturbations times the fraction of time those perturbations are felt, as in eq. (3.3). However here the first order term is the sum of a large number of random uncorrelated terms, and so is Gaussianly distributed over realizations of the perturbation. The mean of this distribution is zero since the perturbation is randomly made contact to contact:

$$\overline{\delta \Delta F^\ddagger} = \sum_i^M \overline{Q_i \delta \epsilon_i} = M Q \overline{\delta \epsilon} = 0, \tag{3.20}$$

i.e. $\overline{\delta \epsilon} = (1/M) \sum_i^M \delta \epsilon_i = 0$, because the native energy is unchanged [83]. The standard deviation

$$\sqrt{\overline{(\delta \Delta F^\ddagger)^2}} = \sqrt{M Q (1 - Q)} b \tag{3.21}$$

scales like \sqrt{N} since $M = zN$. Therefore the first order term in (3.17) will be $\pm \text{const.} \times N^{1/2}$. Here we've let the individual contact variance $\overline{\delta \epsilon_i^2} = b^2$. Similar arguments of the effects of heterogeneity on the barrier were considered in [84].

On the other hand, the second order term in (3.17) is proportional to $\langle \delta V^2 \rangle$ and scales like N and is always negative. By the reasoning in eq. (3.19) the average, over realizations of native disorder, of the thermal fluctuation is

$$\overline{\langle V^2 \rangle} - \langle V \rangle^2 = \sum_{i,j=1}^M \overline{\delta \epsilon_i \delta \epsilon_j} \overline{[\langle \delta_i \delta_j \rangle - \langle \delta_i \rangle \langle \delta_j \rangle]}. \tag{3.22}$$

Since the perturbations are independent of each other the cross terms in the sum vanish: $\overline{\delta \epsilon_i \delta \epsilon_j} = \overline{\delta \epsilon_i^2} \delta_{ij} = b^2 \delta_{ij}$, and

$$\overline{\langle V^2 \rangle} - \langle V \rangle^2 = \sum_{i=1}^M b^2 \overline{Q_i (1 - Q_i)}, \tag{3.23}$$

where the last equality follows from the fact that the fluctuations of particles obeying Fermi-Dirac statistics (c.f. eq. 4.35) obey the property $\langle \delta_i^2 \rangle - \langle \delta_i \rangle^2 = \langle \delta_i \rangle (1 - \langle \delta_i \rangle)$. The sum in (3.23) has the form of M positive terms and thus scales extensively ($\sim M$) with the size of the system as opposed to the first order term. Thus the free energy change due to random perturbations in the native energies is negative in the thermodynamic limit. Since native contacts are less formed in the unfolded state than in the transition state, the change in barrier height is also negative in the thermodynamic limit.

That higher order terms do not reverse the trend in barrier height can be ensured by the Peierls-Bogoliubov inequality $F \leq F_o + \langle V \rangle_o$ where F_o is the free energy in absence of the random component and V is the random part of the Hamiltonian averaged over the unperturbed states, which is just the first order term in eq. (3.17). Thus the transition state free energy (per volume) $F(Q^\ddagger)/N$ is always less than the unperturbed free energy $F_o(Q^\ddagger)/N$ in the thermodynamic limit, and since $F(0) \cong F_o(0)$ in the unfolded state, the barrier is always lowered.

3.C. Distributing native energies uniformly in a well-designed protein maximizes the thermal entropy

If we consider for illustration that native energies are chosen from a distribution which is the independent product of Gaussians

$$P(\{\epsilon_i\}) \approx \prod_{i=1}^M \exp\left(-\frac{(\epsilon_i - \bar{\epsilon})}{2b^2}\right), \quad (3.24)$$

then the native energies will typically fluctuate around their average $\bar{\epsilon}$ on a scale b , with the set of energies $\epsilon_i = \bar{\epsilon}$ being the most likely distribution. We are ignoring for now any constraints on the native energies that might be present in real proteins, e.g. for functional requirements. We now show that this distribution of native energies maximizes the thermal entropy at any degrees of nativeness, for well-designed proteins.

The entropy at Q is given by

$$S(Q) = - \sum_{\alpha} p_{\alpha} \ln p_{\alpha} \quad (3.25)$$

where the sum is over all states at Q , and p_{α} is the probability that state α is occupied from the ensemble of states at Q . We approximate a well-designed protein by a $G\bar{o}$ model. Then if all the native energies are equal ($\epsilon_i = \bar{\epsilon}$), all states at Q have the same energy $E_{\alpha} = QE_N$. Then the partition function Z is $\Omega(Q) \exp(-QE_N/T)$, where $\Omega(Q)$ is the total number of configurational states at Q . Then the probability any state is occupied is $1/\Omega(Q)$, and the thermal entropy becomes

$$S(Q) = \ln \Omega(Q) \quad (3.26)$$

which is the configurational entropy- the largest the thermal entropy can possibly be. This result is recovered again using the general free energy functional theory in section 5.5.C.2, and can be seen in fig. 10.

It should be noted that even though the entropy at the bottleneck is maximized for this choice of energies, the barrier is not minimized, and in fact may be lowered further by the addition of energetic heterogeneity as described above.

4. FREE ENERGY FUNCTIONAL

In this section we derive the free energy functional to be used in the main analysis. This should solidify the concepts outlined in the previous section regarding the effects of heterogeneity on the folding mechanism. We first show how the functional is related to the Hamiltonian, as in section 2.2.A. Then in section 4.4.B the entropic terms present in the functional are derived. In 4.4.C the thermal contact probabilities are obtained by minimizing the free energy functional.

4.A. Obtaining the functional from a Hamiltonian

We can motivate the form of the free energy functional from landscape arguments, i.e. by considering energy distributions of states with structural similarity to the native. Consider a contact Hamiltonian \mathcal{H} of the form

$$\mathcal{H}(\{\Delta_{\alpha\beta}\} | \{\Delta_{\alpha\beta}^N\}) = \sum_{\alpha < \beta} \epsilon_{\alpha\beta}^N \Delta_{\alpha\beta} \Delta_{\alpha\beta}^N + \epsilon_{\alpha\beta} \Delta_{\alpha\beta} (1 - \Delta_{\alpha\beta}^N) \quad (4.1)$$

which gives the energy of a particular configuration defined by the set of contact interactions $\{\Delta_{\alpha\beta}\}$. This Hamiltonian gives energy $\epsilon_{\alpha\beta}^N$ to the contacts which are native contacts, and energy $\epsilon_{\alpha\beta}$ to non-native contacts. We embody the principle of minimum frustration [24] by making the mean of the distributions from which native contact energies are chosen be lower than the mean of the distribution for non-native contact energies. Native contacts may also have a smaller variance, depending on the effective number of effective letters in the sequence. The energies in (4.1) are internal free energies of spatially short-ranged interaction between effective monomeric units, after averaging over side chain and solvent degrees of freedom. The double sum is over residue indices, and $\Delta_{\alpha\beta} = 1$ if residues α and β are in contact in a configuration, $\Delta_{\alpha\beta} = 0$ otherwise. $\Delta_{\alpha\beta}^N = 1$ if these residues are also in contact in the *native* configuration, and $\Delta_{\alpha\beta}^N = 0$ otherwise. $\epsilon_{\alpha\beta}^N$ and $\epsilon_{\alpha\beta}$ are again the energies of native and non-native contacts respectively.

We obtain the thermodynamics for this system by considering statistical properties of an ensemble of partially native states. Once the density of states $n(E | \{Q_i\})$ is known the thermodynamics at temperature T can be obtained. We obtain a statistical average of $n(E | \{Q_i\})$ from a knowledge of the overall number of

partially native states, and the probability each of these states has a given energy. A similar derivation for a homogeneous order parameter Q was calculated in [61]. The probability a configuration with a particular set of native contacts $\{\Delta_{\alpha\beta}\Delta_{\alpha\beta}^N\}$ has energy E , given the native state has energy E_N , is given by

$$P(E|E_N, \{\Delta_{\alpha\beta}\Delta_{\alpha\beta}^N\}) = \langle \delta[E - \mathcal{H}\{\Delta_{\alpha\beta}\}] \delta[E_N - \mathcal{H}\{\Delta_{\alpha\beta}^N\}] \rangle_{non-nat} \quad (4.2)$$

where the averaging is over the non-native contact coupling energies,

$$\langle \dots \rangle_{non-nat} = \int \prod_{non-nat} P(\epsilon_{\alpha\beta}) d\epsilon_{\alpha\beta}.$$

Residual features in the folding mechanism may be present due to non-self-averaging effects of non-native interactions, resulting in phenomena such as “off-pathway” intermediates. We smooth over such phenomena with the above averaging, leaving only an average non-native background field, while native interactions are explicitly retained. Thus “on-pathway” intermediates, or fluctuations in the free energy landscape as in fig. 5 due to native structural or energetic heterogeneity are retained in this procedure. Note $\mathcal{H}\{\Delta_{\alpha\beta}^N\}$ is just the sum of the native interaction energies. Averaging the Fourier-transformed delta functions over non-native interactions chosen from a Gaussian distribution,

$$P(\epsilon_{\alpha\beta}) = \frac{1}{(2\pi b^2)^{1/2}} \exp\left(-\frac{\epsilon_{\alpha\beta}^2}{2b^2}\right)$$

results in

$$P(E|E_N, \{\Delta_{\alpha\beta}\Delta_{\alpha\beta}^N\}) = \frac{1}{(2\pi Mb^2(1-Q))^{1/2}} \exp\left(-\frac{(E - \sum_i \epsilon_i Q_i)^2}{2Mb^2(1-Q)}\right) \quad (4.3)$$

where the sum over native contacts $\sum_{\alpha\beta} \epsilon_{\alpha\beta}^N \Delta_{\alpha\beta} \Delta_{\alpha\beta}^N$ is written in the shorthand single index notation $\sum_i \epsilon_i Q_i$, i.e. $Q_i \equiv \Delta_{\alpha\beta} \Delta_{\alpha\beta}^N$. Here $Q_i = 0, 1$ but in the free energy functional, fractional values are allowed as in the derivation of eq. (2.4) (the entropy per spin would be zero if only integer values of the spin degree of freedom were allowed). We will see that the thermal values of the contact probabilities $Q_i^* = \langle \Delta_{\alpha\beta} \Delta_{\alpha\beta}^N \rangle_T$ are the fractional values that minimize the functional (c.f. eq. (4.35) in sect. 4.4.C).

When the log density of states $\log n(E|\{Q_i\})$ is large, it can be replaced by the disorder-averaged number $\Omega(\{Q_i\})P(E|E_N, \{Q_i\})$, since the relative fluctuations in the number die off as $M^{-1/2}$ for uncorrelated disorder:

$$\log n(E|\{Q_i\}) \approx S(\{Q_i\}) - \frac{(E - \sum_i \epsilon_i Q_i)^2}{2Mb^2(1-Q)}. \quad (4.4)$$

The term $S(\{Q_i\})$ is the configurational entropy, discussed below. The thermal energy $E(T|\{Q_i\})$ is obtained from the density of states above through $\partial \log n(E)/\partial E = T^{-1}$:

$$E(T|\{Q_i\}) = \sum_i \epsilon_i Q_i - \frac{Mb^2}{T}(1-Q). \quad (4.5)$$

This procedure is applicable in the high temperature regime when the number of states occupied at such temperatures is large. The energy consists of an integration over an energy density i.e. by an energy per contact times the probability that contact is made, $\epsilon_i Q_i$, summed over all contacts, minus a term corresponding to a lowering of the thermal energy due to the net effect of non-native traps. Substituting (4.5) into (4.4) gives the thermal entropy

$$S(T|\{Q_i\}) = S(\{Q_i\}) - \frac{Mb^2}{2T^2}(1-Q), \quad (4.6)$$

which consists of the entropy of the polymer chain subject to the geometric constraints $\{Q_i\}$ of contact formation, $S(\{Q_i\})$, and a lowering term due to the presence of non-native traps (fluctuations in Boltzmann weights due to the fluctuations in state energies reduces the effective total number of states occupied). The temperature dependence of $S(\{Q_i\})$ appears through the implicit temperature dependence of the contact probabilities Q_i (see eq. (4.35)).

At this point, since no exact solution for the entropy of a three-dimensional polymer containing topological constraints is known, we must either resort to an exact solution of an approximate, idealized model system, or an approximate phenomenological treatment of the real, exact system. We choose the latter approach for the theory, and the former approach in the lattice simulations. While still an approximation, the entropy we derive captures the same quantitative effects we see in the simulations, which of course contains an exact computation of the entropy for the idealized lattice model. When computing the entropy in the contact representation, we must calculate how much entropy the unconstrained polymer has, Ns_o , how much polymer entropy is lost to form a set of contacts consistent with an overall fraction Q of native structure, $\mathcal{S}_{\text{BOND}}(\{Q_i\}|\{\ell_i\})$, and how much “mixing” entropy is contained in the diversity of contact patterns consistent with that overall fraction Q of native structure, $\mathcal{S}_{\text{ROUTE}}(\{Q_i\})$:

$$S(\{Q_i\}) = Ns_o + \mathcal{S}_{\text{ROUTE}}(\{Q_i\}) + \mathcal{S}_{\text{BOND}}(\{Q_i\}|\{\ell_i\}) . \quad (4.7)$$

These contributions are discussed in detail in section 4.4.B.

The free energy functional at temperature T and nativeness Q is written as $E - TS$ in terms of the field $\{Q_i\}$, using eq.s (4.5), (4.6) and (4.7) :

$$\begin{aligned} F(T|\{Q_i(Q)\}|\{\epsilon_i\},\{\ell_i\}) &= \sum_i \epsilon_i Q_i - T\mathcal{S}_{\text{ROUTE}}(\{Q_i\}) - T\mathcal{S}_{\text{BOND}}(\{Q_i\}|\{\ell_i\}) \\ &+ \bar{E}(Q,\eta) - NTs_o - \frac{Mb^2}{2T}(1-Q) . \end{aligned} \quad (4.8)$$

The terms depending on $\{Q_i\}$ in eq. (4.8) involve integrations over the native density field $\{Q_i\}$, while the remaining terms depend only on the uniform “background field” Q . We have included a mean energy $\bar{E}(Q,\eta)$ dependent on Q and total packing fraction η , the total configurational entropy $Ns_o = N \ln \nu$, where ν is the number of configurations per residue in the unconstrained polymer, and the correction to the free energy due to non-native ruggedness $-\Delta E^2(Q)/2T$. These uniform terms are not central to our main analysis, which considers specifically the effects of native heterogeneity in structure and contact energy.

We note in passing that for the ensemble of sequences with only overall stability $\sum_i \epsilon_i = E_N$ specified, rather than the whole distribution $\{\epsilon_i\}$ as in eq. (4.8) above, the non-native ruggedness decreases with Q as $\sim (1-Q^2)$ [61], rather than as $(1-Q)$ as above. This results from averaging over the native coupling energies under the constraint $\sum_i \epsilon_i = E_N$.

The native stability gap is composed of a sum of 2-body interaction energies between M pairs of native residues. Cooperative contributions to the energy function [61, 85] necessary for *de novo* prediction [85, 86] and accurately representing barriers [61, 62] are not studied here, since native stability is present *a priori* in the free energy of our model, and thus we focus specifically on the properties of already well designed sequences to a given structure, for which cooperative effects should induce quantitative but not qualitative changes in the results presented here.

For a Gō-like set of interactions, collapse and folding occur simultaneously. \bar{E} in eq. (4.8) can then be set to zero since all energetic contributions $\sum_i Q_i \epsilon_i$ are from native contacts. At the other extreme, if there is no change in density with folding and the total number of contacts of any kind is a constant, the term $\sum_i Q_i \epsilon_i$ can be interpreted as the *extra* energy native contacts get. Then \bar{E} is a constant, which again has no effect on the free energy. In an intermediate regime there is some non-native density coupling to progress along the folding reaction coordinate [61]. Since this subtle effect is secondary to and unnecessary for the analysis below, we ignore it and treat \bar{E} as a constant.

4.B. Entropic Terms

If we imagine the ensemble of configurations that have a given amount of order, say a given number MQ of native contacts, then within this ensemble there are a multiplicity of sub-ensembles of states having different sets of MQ contacts, which we identify as a measure of the number of distinct routes in folding to the native state. Each sub-ensemble contains many states corresponding to the entropy of the disordered polymer around the particular native core (e.g. see fig. 6). We define the entropy that corresponds to the degeneracy of contact patterns having functional order $\{Q_i(Q)\}$ as $\mathcal{S}_{\text{ROUTE}}(\{Q_i(Q)\})$ ($\mathcal{S}_{\text{ROUTE}} > 0$), and the configurational entropy lost from the coil state to induce the ordering specified by $\{Q_i\}$ as $\mathcal{S}_{\text{BOND}}(\{Q_i\}|\{\ell_i\})$ ($\mathcal{S}_{\text{BOND}} < 0$).

4.B.1. Route Entropy

In capillarity models of nucleation [87], $\mathcal{S}_{\text{ROUTE}}$ corresponds to the log of the translational partition function [88–90] which scales logarithmically with system size, plus the entropy of surface fluctuations of droplets of a given size [91, 92] which correspond to logarithmic terms in the expansion of the free energy density. This entropy is small compared to the total conformational entropy, however at the spinodal where $F(Q)$ becomes downhill (e.g. long-dashed curves in fig. 11), the nucleus is of small amplitude and highly ramified [70, 93]. In this regime the droplet structure is percolative as in spinodal decomposition of binary fluids, and the capillarity approximation is poor. Field-theoretic descriptions for the structure of the droplet are typically used in this regime [94, 95]. Binary fluid approximations to the route entropy in proteins which scale extensively with system size have been used in this limit [34, 44, 45, 61, 71, 96, 97]. The amount of route diversity in folding has also been analyzed in terms of the Shannon entropy [98], which is similar in spirit to the following treatment [43]. We make no capillarity or spinodal assumptions, and treat the route entropy $\mathcal{S}_{\text{ROUTE}}(\{Q_i\})$ as a fairly simple modification of the entropy of a binary fluid mixture [82]:

$$\exp \mathcal{S}_{\text{ROUTE}}^o(Q) = \frac{M!}{MQ!(M-MQ)!} \cong (\Omega_i^o)^M \quad (4.9)$$

$$\Omega_i^o = Q^{-Q} (1-Q)^{-(1-Q)} \quad (4.10)$$

which we interpret here as the product of the complexities per contact Ω_i^o and is readily generalized to the case where the complexities are not all equal: $\exp \mathcal{S}_{\text{ROUTE}}^o(\{Q_i\}) \Rightarrow \prod_{i=1}^M Q_i^{-Q_i} (1-Q_i)^{-(1-Q_i)}$, as in eq. (2.4). The principle modification introduced here for proteins is that, due to chain connectivity, as contact density increases, there is less sterically allowed space for a monomer to move around when one of its constraining contacts is broken. Thus not all $M!/MQ!(M-MQ)!$ contact patterns have an entropy $\approx Ns_o + \mathcal{S}_{\text{BOND}}$. In other words making some native contacts forces spatially nearby contacts to be made because the corresponding monomers are forced to be in each other's proximity. So there is a reduction from the putative complexity $(\Omega_i^o)^M$ since not all M contacts are independently contributing to mixing, with several contact patterns corresponding to the same constrained state. Here we remove this degeneracy by dividing out the $(\Omega_i^o)^{Ma(\{Q_i\})}$ states that have been overcounted. Making a mean-field approximation for the local field around contact i which reduces its complexity, $\sum_{\alpha \neq \beta} Q_{\alpha\beta} / \sum_{\alpha \neq \beta} (1) \simeq Q$, the new total complexity is $\prod_{i=1}^M \Omega_i^{[1-a(Q)]}$. Here $a(Q)$ is a monotonically increasing function of Q , from $a(Q \rightarrow 0) = 0$ to $a(Q \rightarrow 1) = 1$, since a nearly fully constrained polymer has all its entropy on the surface, making the mixing entropy per monomer negligible in the thermodynamic limit. We introduce the form $a(Q) = Q^\alpha$ with α a parameter determined by the best fit to the lattice data (see fig.s 7 and 13 and table I). The route entropy appearing in eq. (4.8) then becomes [43]:

$$\mathcal{S}_{\text{ROUTE}}(\{Q_i\}) = \log \prod_{i=1}^M \Omega_i^{\lambda(Q)} = \lambda(Q) \sum_{i=1}^M [-Q_i \ln Q_i - (1-Q_i) \ln (1-Q_i)] \quad (4.11)$$

$$\lambda(Q) \equiv 1 - Q^\alpha \quad (4.12)$$

The factor $\lambda(Q)$ measures the entropy reduction due to the coupling of chain connectivity with the native topology under study. The power α in $\lambda(Q)$ should be a decreasing function of the persistence length, and also of system size N , since for larger systems more polymer is buried and thus more strongly constrained by surrounding contacts. Fluctuations in contact probabilities Q_i will lower the route entropy (see eq. (4.33) and also figure 13). An alternative derivation for the route entropy in a protein is given in Appendix B.

4.B.2. Bond Entropy

The calculation of the total entropy lost due to contact formation is rendered difficult because the entropy loss of a given contact depends not only on the contact's sequence-length or bare loop-length ℓ_i , but also on the configuration of contacts $\{Q_i\}$ already present when the contact is formed. In spite of this difficulty some general statements can still be made, as follows.

If we make the assumption that the entropy loss to form contact i depends explicitly only on the sequence length of contact i , as well as the full contact pattern present $\{Q_i\}$, then the most general form for the change in entropy due to contact formation, to go from configurations having one set of Q_i 's parameterized in terms of a variable t , $\{Q_i(t_o)\}$, to another state having $\{Q_i(t_f)\}$, is

$$\mathcal{S}_{\text{BOND}}(\{Q_i(t_f)\}|\{Q_i(t_o)\}) = \sum_i \int_{t_o}^{t_f} \mathcal{D}Q_i(t) s_i(\ell_i, \{Q_j(t)\}) . \quad (4.13)$$

Here $s_i(\ell_i, \{Q_j(t)\})$ is the entropy loss to form contact i having sequence separation ℓ_i , in the presence of the contact pattern $\{Q_j(t)\}$, which is itself parameterized through t [99]. Each $s_i(\ell_i, \{Q_j(t)\})$ in eq. (4.13) is functionally integrated along the M -dimensional path specified by $\{Q_i(t)\}$. However the entropy as a function of the set $\{Q_i\}$ must be a state function, meaning that the value of the integral depends only on the end points and not on the path taken. The condition for path independence is obtained as follows. We can envision a small subsection of the M -dimensional path as traversing a hypercube of volume $\prod_{i=1}^M \delta Q_i$. Then path independence means the entropy increment $\mathcal{S}_{\text{BOND}}(\{Q_i\}|\{Q_i + \delta Q_i\})$ is independent of the order the edges are traversed in going from $\{Q_i\}$ to $\{Q_i + \delta Q_i\}$. Consider two possible paths labeled (1) and (2) along two of these coordinates $\{Q_i, Q_j\}$, as shown in fig. 8. Along path (1), the entropy change to second order in δQ is

$$\begin{aligned} \mathcal{S}_{\text{BOND}}^{(1)} &= \int_{Q_i}^{Q_i + \delta Q_i} \delta Q'_i s_i(\ell_i, Q'_i, Q_j) + \int_{Q_j}^{Q_j + \delta Q_j} \delta Q'_j s_j(\ell_j, Q_i + \delta Q_i, Q'_j) \\ &\cong s_i(\ell_i, Q_i, Q_j) \delta Q_i + s_j(\ell_j, Q_i, Q_j) \delta Q_j + \frac{\delta Q_i^2}{2} \frac{\partial s_i}{\partial Q_i}(\ell_i, Q_i, Q_j) + \frac{\delta Q_j^2}{2} \frac{\partial s_j}{\partial Q_j}(\ell_j, Q_i, Q_j) \\ &\quad + \delta Q_i \delta Q_j \frac{\partial s_j}{\partial Q_i}(\ell_j, Q_i, Q_j) \end{aligned} \quad (4.14)$$

while along path (2) the entropy change is the same as expression (4.14) except that the last term is replaced by $\delta Q_i \delta Q_j \frac{\partial s_i}{\partial Q_j}(\ell_i, Q_i, Q_j)$. For these two expressions to be equal

$$\frac{\partial s_j}{\partial Q_i}(\ell_j, \{Q_k\}) = \frac{\partial s_i}{\partial Q_j}(\ell_i, \{Q_k\}) \quad \text{for } i \neq j . \quad (4.15)$$

For M dimensions, it follows that eq. (4.15) holds for all pairs (i, j) , yielding $M(M-1)/2$ nontrivial constraints on the form of the configurational entropy loss at each value of Q .

When the entropy loss satisfies eq. (4.15), the total entropy difference only depends on the initial and final states and can be rewritten as

$$\mathcal{S}_{\text{BOND}}(\{Q_i^f\}|\{Q_i^o\}) = \sum_i \int_{Q_i^o}^{Q_i^f} dQ_i s_i(\ell_i, \{Q_j\}) . \quad (4.16)$$

Now we seek an approximate formula for s_i that satisfies eq. (4.15). In forming a contact i from the unconstrained molten globule or coil state, the segment of polymer loses the entropy of a free chain with the length of that segment, $s_i(\ell_i, \{Q_j\} \cong \{0\}) = \ln(a/\ell_i)^{3/2}$ where a is a Q independent constant related through a sum rule to polymeric properties (see eq. (4.25)). However “zippering up” contacts formed in a nearly fully constrained polymer cost almost no entropy: $s_i(\ell_i, \{Q_j\} \approx \{1\}) \cong 0$. To account for this we introduce an effective loop length $\ell_{\text{EFF}}(\ell_i, \{Q_j\})$ into $s_i(\ell_i, \{Q_j\}) = \ln(a/\ell_{\text{EFF}})^{3/2}$. We ignore here possibly important changes in the power of the ideal chain exponent $3/2$, since it becomes cumbersome to incorporate an exponent dependent on $\{Q_i\}$ and to simultaneously satisfy eq. (4.15).

Because of the path independence of the configurational entropy loss $\mathcal{S}_{\text{BOND}}(\{Q_i^f\}|\{Q_i^o\})$, the change in entropy for a small change in one of the contacts $Q_i^f \rightarrow Q_i^f + \delta Q_i$ is simply the integrand evaluated at the upper limit:

$$\frac{\partial \mathcal{S}_{\text{BOND}}}{\partial Q_i}(\{Q_j^f\}|\{Q_j^o\}) = s_i(\ell_i, \{Q_k^f\}) \quad (4.17)$$

which can be shown from eqs. (4.15) and (4.16) by using the definition of the derivative.

In this paper we satisfy eq. (4.15) with the following ansatz for the functional form of ℓ_{EFF} :

$$\ell_{\text{EFF}}(\ell_i, \{Q_k\}) = f(\ell_i) g(\{Q_k\}) = f(\ell_i) g\left(\frac{1}{M} \sum_k Q_k\right) \quad (4.18)$$

so that the loop length is decreased by a function of the mean of the contact density field, $g(Q)$. This is in the spirit of the Hartree ansatz in the one-electron theory of metals, where electrons interact only through an averaged field. The condition $\ell_{\text{EFF}}(\ell_i, Q=0) = \ell_i$ gives $f(\ell_i) = \ell_i$ and $g(0) = 1$. The condition that $\ell_{\text{EFF}}(\ell_i, Q=1) \approx 1$ gives $g(1) \approx 1/\bar{\ell}$ (since $g(Q)$ cannot depend on ℓ_i), where $\bar{\ell} = (1/M) \sum_i \ell_i$. To approximate the Q dependence of ℓ_{EFF} we note that the probability of a monomer being constrained at Q is roughly Q under the assumption of a uniform contact probability. Then given a chain of unbonded monomers, the probability of it being length L is then $p_L = Q(1-Q)^{L-1}$. So the average length of strings of unbonded monomers at Q is then $\bar{L} = \sum_L L p_L / \sum_L p_L \cong 1/Q$, which can be interpreted roughly as the total length of polymer N over the total number of bonds $\approx NQ$ [100], or the total length over the total number of constrained monomers. We approximate the effective loop length at Q , $\ell_{\text{EFF}}(\ell_i, Q)$, in the same way by dividing the total loop length ℓ_i by the number of bonded residues in the loop (or the approximate number of bonds in the loop) $\cong \bar{\ell}Q$, so that finally

$$s_i(\ell_i, \{Q_k\}) \approx \frac{3}{2} \ln \left(\frac{a}{\ell_{\text{EFF}}(\ell_i, Q)} \right) \quad (4.19)$$

$$\ell_{\text{EFF}}(\ell_i, Q) \approx \frac{\ell_i}{(\bar{\ell} - 1)Q + 1} \quad (4.20)$$

Note ℓ_{EFF} has the mean-field behavior for large ℓ_i and also has the right limiting behavior as $Q \rightarrow 0$ and $Q \rightarrow 1$. Eq.s (4.20) and (4.19) are accurate for weak dispersion in loop lengths; for larger values of $\delta\ell_i$ they must be modified (see comments after eq. (4.29)).

Expressions (4.16) and (4.19) reduce to the Flory form for the configurational entropy loss in the mean field limit [96, 100, 101] when $\ell_i = \bar{\ell}$ and $Q_i = Q$. Then eq. (4.16) becomes

$$\mathcal{S}_{\text{BOND}}^{(\text{MF})}(Q|0) = \int_0^Q dQ' M \ln \left(\frac{a [1 + (\bar{\ell} - 1) Q']}{\bar{\ell}} \right)^{3/2}, \quad (4.21)$$

which can be interpreted as a summation of entropy losses from 0 to Q :

$$\begin{aligned} \mathcal{S}_{\text{BOND}}^{(\text{MF})}(Q|0) &= \sum_{Q'=\Delta Q}^Q \Delta S(Q') = \sum_{Q'=\Delta Q}^Q \ln \frac{\Omega(Q')}{\Omega(Q' - \Delta Q)} \\ &= \ln \left(\frac{\Omega(\Delta Q)}{\Omega(0)} \frac{\Omega(2\Delta Q)}{\Omega(\Delta Q)} \cdots \frac{\Omega(Q)}{\Omega(Q - \Delta Q)} \right) = \ln \frac{\Omega(Q)}{\Omega(0)} \\ &= S^{(\text{MF})}(Q) - S^{(\text{MF})}(0). \end{aligned}$$

When $\bar{\ell}Q \gg 1$, eq. (4.21) gives

$$\frac{\mathcal{S}_{\text{BOND}}^{(\text{MF})}}{M}(Q|0) = \frac{3Q}{2} (\ln a - 1 + \ln Q) \quad (4.22)$$

which is essentially the Flory result derived earlier in the mean-field limit.

In the presence of heterogeneity, equations (4.16) and (4.19) give

$$\begin{aligned} \mathcal{S}_{\text{BOND}}(\{Q_i\}|0) &= \frac{3}{2} M Q \ln a - \sum_{i=1}^M Q_i \ln \ell_i + \sum_{i=1}^M \int_0^{Q_i} dQ'_i \ln \left[1 + \frac{\bar{\ell} - 1}{M} \sum_k Q_k \right] \\ &= \frac{3}{2} M \left(Q (\ln a) - \frac{1}{M} \sum_i Q_i \ln \ell_i - Q + \frac{[1 + (\bar{\ell} - 1)Q]}{\bar{\ell} - 1} \ln [1 + (\bar{\ell} - 1)Q] \right) \end{aligned} \quad (4.23)$$

where the last integral can be done by charging up each Q_i one at a time (in any order) to its value at Q , i.e. the integral is $\sum_i \int_0^{Q_i} dQ'_i \ln \left[1 + \frac{\bar{\ell} - 1}{M} (\sum_{j < i} Q_j + Q'_i) \right]$. This gives an expression identical to the mean-field result for this term, since the integrand only depends on Q and is integrated up to each $Q_i(Q)$.

Because the free energy of the native state $F(\{1\}|\{\epsilon_i\}, \{\ell_i\})$ is E_N (c.f. eq. (4.8)), all the polymer entropy is lost upon folding in the model. Therefore there is a sum rule for the entropy loss,

$$\mathcal{S}_{\text{BOND}}(\{1\}|0) = \sum_{i=1}^M \int_0^1 dQ_i s_i(\ell_i, \{Q_j\}) = -N \ln \nu = -N s_o, \quad (4.24)$$

which, using eq. (4.23), determines the coefficient a in the entropy of bond formation:

$$\ln a(\nu, \{\ell_i\}) = -\frac{2s_o}{3z} + 1 + \overline{\ln \ell} - \frac{\bar{\ell}}{\bar{\ell}-1} \ln \bar{\ell}. \quad (4.25)$$

The coefficient a depends on the distribution of ℓ_i as well as the entropy per monomer s_o . Using (4.25) and (4.23), the final expression for the entropy loss arising from contact formation is

$$\mathcal{S}_{\text{BOND}}(\{Q_i\}|0) = \mathcal{S}_{\text{MF}}(Q, \bar{\ell}) - \frac{3}{2}M \langle \delta Q \delta \ln \ell \rangle \quad (4.26)$$

where the first term in (4.26) is the mean-field entropy loss

$$\mathcal{S}_{\text{MF}}(Q, \bar{\ell}) = -QN s_o - \frac{3}{2}MQ \frac{\bar{\ell} \ln \bar{\ell}}{\bar{\ell}-1} + \frac{3}{2}M \frac{1}{\bar{\ell}-1} [1 + (\bar{\ell}-1)Q] \ln [1 + (\bar{\ell}-1)Q] \quad (4.27)$$

and the second term in (4.26) is the change in entropy loss due to fluctuations (again the notation $\langle X_i \rangle \equiv \overline{X} \equiv \frac{1}{M} \sum_i X_i$ is used):

$$M \langle \delta Q \delta \ln \ell \rangle = \sum_i (Q_i - Q) (\ln \ell_i - \overline{\ln \ell}). \quad (4.28)$$

From inspection of eq.s (4.26-4.28) we can confirm that $\mathcal{S}_{\text{BOND}}(Q=0) = 0$ and $\mathcal{S}_{\text{BOND}}(Q=1) = -N s_o$. When $\bar{\ell}Q \gg 1$, (4.27) reduces to eq.s (4.22), (4.25):

$$\mathcal{S}_{\text{MF}}(Q, \bar{\ell} \gg 1) \approx -QN s_o + \frac{3}{2}zNQ \ln Q, \quad (4.29)$$

which has lost the information about the mean loop length and only retained information about the total chain length N , as in the Flory mean-field theory. The first term in (4.27) or (4.29) is the loss in entropy to constrain a given fraction of the protein and is linear in Q . The remainder in (4.27) or (4.29) is the extra entropy loss this constraint induces on the remaining free parts by pinning down regions of the polymer chain. The analogous quantity in the capillarity theory is the surface entropy cost in forming a nucleus of folded structure [84, 102]. In capillarity theories, the surface entropy cost scales like $N^{2/3}$, whereas in mean-field theories it scales like N . Eq. (4.27) can be thought of as a generalization of eq. (4.29) to finite mean return length $\bar{\ell}$ for a finite-sized system, and eq. (4.26) can be thought of as generalizing (4.27) to include fluctuations in the return length.

The effect of fluctuations in (4.26) is typically to increase the bond entropy of partially native states. The trend in the folding barrier with heterogeneity results from the interplay of this effect with the effects of fluctuations on the route entropy and native energetic fluctuations. The magnitude of the effect scales extensively with the size of the system. To illustrate, recall that for a Gō model the total entropy at Q is $N s_o + \mathcal{S}_{\text{ROUTE}}(\{Q_i\}) + \mathcal{S}_{\text{BOND}}(\{Q_i(Q)|0\})$ (c.f. eq.s (4.6) and (4.7)). Thus if we look at loops longer than the average ($\ell_i > \bar{\ell}$, and since the log function is concave down, $\ln \ell_i > \overline{\ln \ell}$), then they are less likely to be formed (c.f. eq. 4.35), so that $Q_i < Q$ and the second term in (4.26) is negative, thus raising the bond entropy. If $\ell_i < \bar{\ell}$, $Q_i > Q$ and the effect is the same. The halo entropy of the system $N s_o + \mathcal{S}_{\text{BOND}}(\{Q_i(Q)|0\})$, or Flory entropy as we refer to it later, increases when we relax the condition that all contacts must be equally probable, and allow differences in contact probability based on their entropic likelihood (see fig. 15).

From (4.29) it can be seen that there is an entropy crisis ($\mathcal{S}_{\text{MF}} < 0$) at values of $Q < 1$ when $2s_o/3z \lesssim 1$. This is essentially because in the mean field approximation contacts are shared equally between residues; only one contact is needed to constrain a residue, however there may be more than one contact per residue. The increase in entropy from heterogeneity alleviates (but not necessarily eliminates) this problem. The route entropy described above in section (4.4.B.4.B.1) further increases the total entropy. However if there is a crisis, then at Q values higher than that where the entropy crisis occurs, the mean field description is no longer valid. Typical values of the parameters from off-lattice simulations of Chymotrypsin inhibitor or the α -spectrin SH3 domain [39] give $s_o \cong 3.4$, $z \cong 2.4$, $2s_o/3z \cong 0.94$; here the entropy crisis occurs rather late in folding, if at all, because of entropy increase by the above-mentioned effects. At Q values above the crisis, fluctuations from

the mean-field contacts per residue must be accounted for. One way to achieve this is to switch to a residue representation for the entropy: the number of states is counted by considering the combinatorics of strings of residues which are frozen or melted out [61].

On the other hand, eq. (4.19) breaks down for sufficiently large structural heterogeneity. Inspection of (4.19) shows that the entropy loss has the same derivative as a function of Q for all contacts, but the initial values are different. This leads to some problems with the shorter loops for high Q values, which it is worth noting as a word of caution here. The crude way in which the entropy loss for a loop is coupled to the degree of nativeness of the rest of the protein leads to a non-negative entropy loss to close some of the shorter loops near $Q \approx 1$. We resolved this problem by actually truncating the entropy loss formula for the shorter loops when they reached a value of zero. Putting eq. (4.25) into (4.19), letting $\bar{\ell}Q \gg 1$, and expanding to first order in $\delta\ell/\bar{\ell}$ (weak dispersion limit) we obtain the approximate value of Q where the entropy loss crosses zero, namely $Q_v \approx 2s_o/3z + \delta\ell_i/\bar{\ell}$. When $\delta\ell_i = 0$ this is consistent with the Flory analysis above, however when $\delta\ell_i < 0$ (shorter loops) Q_v is decreased. We truncate the entropy formula at zero for $Q > Q_v$.

As a simple illustration, consider a structure whose loop distribution is given by first returns of a self-avoiding walk, $P(\ell) \approx (3/2)\ell^{-5/2}$, and thus from eq. (4.19) $P(s) = \exp(s - s(\ell_i = 1))$, where $s(\ell_i = 1) = 5/2 - (9/4)\ln 3 - s_o/z + (3/2)\ln(1 + 2Q)$ is the entropy of closure for the smallest loops (where the problem is the worst). Using the above values for s_o and z , all s_i are negative until $Q_v \gtrsim 0.76$. Since the barrier peak typically occurs at Q values smaller than this, errors due to truncation would be small for these structures. On the other hand protein structures tend to have distributions with a wider dispersion than the random globule, and in these cases the problem would be worse. Applying the theory to the lattice structure of fig. 1, we must truncate the entropy loss for loops with $\ell_i = 3$ at $Q_{v3} \approx 0.4$ and for loops with $\ell_i = 5$ at $Q_{v5} \approx 0.75$; for all other loops there is no entropy crisis. Numerically there is some quantitative error introduced by this truncation, since in the theory these loops no longer contribute to the total entropy loss above Q_v , whereas in the actual simulation they do. Of course, implementing a cutoff in loop entropy causes the total entropy to deviate from a state function by eq. (4.15). Theories of polymer entropy which take more complete account of correlations should remedy this and are a topic of future work. For now we content ourselves with the Hartree style entropy formulation in eq. (4.19), implementing a cutoff if needed. In general however truncating doesn't qualitatively change trends in the barrier except possibly in pathological cases of limited relevance.

Equations (4.8), (4.11) and (4.26) together give an analytic expression for the free energy for a fast-folding protein which includes heterogeneity in the folding mechanism:

$$F(\{Q_i(Q)\} | \{\epsilon_i\}, \{\ell_i\}) = F_{\text{MF}}(Q, \bar{\epsilon}, \bar{\ell}) + \delta F(\{\delta Q_i\} | \{\delta\epsilon_i\}, \{\delta\ell_i\}) \quad (4.30)$$

where we've written the total free energy in terms of a mean-field term plus a fluctuation due to variations in energy, loop length, and contact probability. In (4.30), F_{MF}/M is the mean-field free energy per monomer [61]:

$$\frac{F_{\text{MF}}}{M} = \bar{\epsilon}Q - T\frac{s_o}{z} - T\frac{\mathcal{S}_{\text{MF}}}{M}(Q, \bar{\ell}) - T\frac{\mathcal{S}_{\text{ROUTE}}}{M}(Q) - \frac{b^2}{2T}(1 - Q) + \frac{\bar{E}}{M} \quad (4.31)$$

with \mathcal{S}_{MF} given by eq. (4.27), and $\mathcal{S}_{\text{ROUTE}}$ given by eq. (4.11) with all $Q_i = Q$. The fluctuation in (4.30) is given by

$$\frac{\delta F}{M}(\{\delta Q_i\} | \{\delta\epsilon_i\}, \{\delta\ell_i\}) = \langle \delta Q \delta \epsilon \rangle + T\lambda(Q) \left\langle Q_i \ln \frac{Q_i}{Q} + (1 - Q_i) \ln \frac{1 - Q_i}{1 - Q} \right\rangle + \frac{3}{2}T \langle \delta Q \delta \ln \ell \rangle \quad (4.32)$$

Equation (4.31) contains 5 adjustable parameters which characterize the system: N, s_o, z, b and \bar{E} , and eq. (4.32) contains 1 adjustable parameter: α in $\lambda(Q)$ of eq. (4.12). Once chosen, these parameters are fixed for the rest of the analysis. We've chosen some values for the parameters in table I to compare with the lattice simulations. All other quantities such as $\bar{\epsilon}, \bar{\ell}, \delta\ell^2$, etc. arise from the structural and energetic distribution of a given protein at overall nativeness Q and temperature T . In our analysis we study trends in the thermodynamics by varying these distributions.

As noted above, the free energy functional consists of an integration over a free energy density whose only information about the surrounding medium is through the average field present (Q): $F = \sum_i f_i(Q_i, Q)$. Explicitly accounting for cooperative entropic effects due to correlations between contacts [34, 45, 103, 104] would be an important extension of the model, and terms that lead to such effects have been introduced into the functional in similar models [34, 45].

We can make connection with the intuitive arguments discussed previously by investigating the effects of heterogeneity on each of the three terms in eq. (4.32). As mentioned above, for longer loops the contact probability is expected to be less than average, and for shorter loops Q_i is expected to be above average. So

relaxing the Q_i values to accommodate this makes the third term in (4.32) negative, lowering the free energy. Also, since the fluctuation δQ_i is expected to be positive when a contact is stronger ($\delta \epsilon_i$ is negative), the first term in (4.32) is negative and the free energy is lowered. Lastly, the second term in eq. (4.32) consists of two terms inside the average which are both concave up, i.e. have a positive second derivative w.r.t. Q_i . Thus the average of the terms is greater than the term evaluated at the average, i.e.

$$\begin{aligned} \left\langle Q_i \ln \frac{Q_i}{Q} \right\rangle &> \langle Q_i \rangle \ln \frac{\langle Q_i \rangle}{Q} = 0 \\ \left\langle (1 - Q_i) \ln \frac{1 - Q_i}{1 - Q} \right\rangle &> (1 - \langle Q_i \rangle) \ln \frac{1 - \langle Q_i \rangle}{1 - Q} = 0, \end{aligned} \quad (4.33)$$

and so the second term in (4.32) is positive. Fluctuations away from uniform ordering raise the terms in the free energy due to route entropy. This effect competes with the two lowering effects above. To find which terms dominate, we find the functional dependence of the contact probabilities Q_i on the energies ϵ_i and entropies s_i in the next subsection, and then investigate the trend on barrier height in section 5.

4.C. The most likely distribution of contact probabilities

Equations (4.30), (4.31), and (4.32) describe the free energy for an arbitrary distribution of contact probabilities $\{Q_i(Q)\}$, subject only to the constraint that the average probability $\langle Q_i \rangle$ is Q . The most likely distribution $\{Q_i^*(Q)\}$ of the contact probabilities $Q_i(Q)$, i.e. the thermal distribution, is obtained by minimizing the free energy $F(\{Q_i(Q) | \{\epsilon_i\}, \{\ell_i\}\})$ subject to the constraint $\sum_i Q_i(Q) = MQ$, i.e. $\delta(F + \mu \sum_j Q_j) = 0$, or

$$\sum_i \left[\frac{\partial}{\partial Q_i} F(\{Q_i\} | \{\epsilon_i\}, \{\ell_i\}) + \mu \right] \delta Q_i = 0 \quad (4.34)$$

for arbitrary and independent variations δQ_i (c.f. the analogous expression eq. (2.5)). Substituting eqs. (4.30), (4.31), and (4.32) into eq. (4.34) yields a Fermi-Dirac distribution for the most probable thermodynamic occupation probabilities $\{Q_i^*\}$ for a given $\{\epsilon_i\}$ and $\{\ell_i\}$:

$$Q_i^*(Q, \{\epsilon_i\}, \{\ell_i\}) = \frac{1}{1 + \exp \left[\frac{1}{\lambda T} (\mu + \epsilon_i - T s_i(\ell_i, Q) - T \lambda' \langle s_{\text{ROUTE}}^o \rangle + \frac{b^2}{2T}) \right]}, \quad (4.35)$$

where $\lambda' = d\lambda(Q)/dQ$ (c.f. eq. 4.12) and $\langle s_{\text{ROUTE}}^o \rangle(Q) = \langle -Q_j \ln Q_j - (1 - Q_j) \ln(1 - Q_j) \rangle$. Thus each probability Q_i^* , referred to below simply as Q_i , is a function of all the $\{Q_j\}$, and must be solved for self-consistently. Non-native ruggedness introduces a term with anomalous $1/T^2$ temperature dependence in the distribution. By the structure of eq. (4.35), all contact probabilities Q_i are between zero and one.

The Lagrange multiplier μ is determined by the constraint $\sum_i Q_i^* = MQ$, and so is a function of Q and the distributions of $\{\epsilon_i\}$ and $\{\ell_i\}$. It can be interpreted as proportional to an effective force along the Q coordinate since

$$\mu = -\frac{1}{M} \frac{\partial F}{\partial Q} \quad (4.36)$$

by the properties of the Legendre transformation (see Appendix A). Thus again since the free energy F is of course a function of Q and the distributions $\{\epsilon_i\}$ and $\{\ell_i\}$, $\mu = -(1/M) \partial F / \partial Q$ is also.

The second variation of $F(\{Q_i\} | \{\epsilon_i\}, \{\ell_i\})$ (neglecting terms of order $\mathcal{O}(1/M)$) is indeed positive

$$\frac{\partial^2 F}{\partial Q_j \partial Q_i} = \lambda T \frac{\delta_{ij}}{Q_i (1 - Q_i)} > 0, \quad (4.37)$$

verifying that the extremal values of Q_i are the ones which minimize $F(\{Q_i\} | \{\epsilon_i\}, \{\ell_i\})$.

5. CHANGING FOLDING MECHANISMS BY TAILORING NATIVE INTERACTION ENERGIES AND ALTERING NATIVE STRUCTURAL MOTIFS

Most single domain proteins most fold over a free energy barrier of a few $k_B T$ at the transition temperature. This barrier is small compared to the total thermal energy in the system, reflecting the exchange of energy

for entropy as a protein folds [61, 105]. However the barrier height can vary significantly depending on which parts of a protein are most stable in the native structure, i.e. how the native energy is distributed throughout the native structure. In section 5.5.A we look at the effects on the thermodynamics when native interactions are changed in a controlled manner. We find that a distribution of native energy which induces a uniform folding mechanism will maximize the barrier. For model systems of small proteins this barrier is about twice as large as the barrier when native energies are uniformly distributed. Increasing heterogeneity in the folding mechanism systematically decreases the folding barrier and may eliminate it entirely, at least in the absence of cooperative interactions. The corresponding folding rate increases, as long as the protein remains well-designed. In section 5.5.B we develop a perturbation expansion of the free energy to incorporate structural as well as energetic heterogeneity, and the effect on the free energy of correlations between them. In 5.5.C we further apply the functional theory to calculate various thermodynamic quantities and compare the results with simulations of the lattice 27-mer, and in 5.5.D we continue the comparison by applying the functional theory to properties of the folding mechanism. In section 5.5.E we show how the folding barrier decreases with the degree of route-like folding in the system, so long as the protein remains well-designed. In 5.5.F we explicitly investigate the kinetics of folding times in the system and find that folding kinetics is well-characterized by the thermodynamic folding barrier. In 5.5.G we illustrate the effect of contact order or mean contact length on the folding barrier in the model. In 5.5.H we investigate the effects of structural variance on a hypothetical ensemble of well-designed protein fold motifs. We find that for fixed average loop length $\bar{\ell}$, native structures that have larger dispersion $\delta\ell$ in the distribution of return lengths tend to have smaller folding barriers. Finally in section 5.5.I we show how native energies can be tuned or native structures can be sought to match a desired free energy potential, which we illustrate for a simple two-state potential as well as a potential with an on-pathway intermediate.

5.A. Energetic heterogeneity for a given structure

First we consider the free energy as a function of Q and the field of energies $\{\epsilon_i\}$, given the field of loop lengths $\{\ell_i\}$. Each contact probability Q_i in the free energy (eq. 4.32) is considered through eq. (4.35) to be a function of Q , its energy, its loop length, and the Lagrange multiplier $\mu(Q, \{\epsilon_j\}, \{\ell_j\})$, which is itself a function of Q and the distributions $\{\epsilon_j\}$ and $\{\ell_j\}$. Thus the free energy depends both implicitly and explicitly on $\{\epsilon_i\}$.

We now seek to relax the values of $\{\epsilon_i\}$, at fixed stability (fixed total native energy)

$$\sum_j \epsilon_j = E_N, \quad (5.1)$$

$$\sum_j \delta\epsilon_j = 0 \quad (5.2)$$

to the distribution $\{\epsilon_i^*(\{\ell_j\})\}$ that extremizes the free energy barrier. Under variations of the energies $\{\delta\epsilon_i\}$ for a given structure $\{\ell_i\}$, the free energy becomes

$$F\{\epsilon_{io} + \delta\epsilon_i\} = F\{\epsilon_{io}\} + \sum_i \left(\frac{\delta F}{\delta\epsilon_i} \right)_{\epsilon_{io}} \delta\epsilon_i + \frac{1}{2!} \sum_{i,j} \left(\frac{\delta^2 F}{\delta\epsilon_i \delta\epsilon_j} \right)_{\epsilon_{io}, \epsilon_{jo}} \delta\epsilon_i \delta\epsilon_j + \dots, \quad (5.3)$$

where $\delta/\delta\epsilon_i$ is the total derivative with respect to ϵ_i . So the distribution $\{\epsilon_i^*(\{\ell_j\})\}$ that extremizes the free energy barrier subject to the constraint eq. (5.1) is the solution of $\delta(\Delta F^\ddagger - p \sum_j \epsilon_j) = 0$, or

$$\sum_i \left[\frac{\delta \Delta F^\ddagger}{\delta\epsilon_i} - p \right] \delta\epsilon_i = 0 \quad (5.4)$$

for arbitrary and independent variations $\delta\epsilon_i$ in the energies. The Lagrange multiplier p imposes the constraint that the total native energy E_N is constant. Changes in the barrier height are roughly equal to changes in the free energy at the barrier peak, since the free energy in the unfolded state $Q_o \approx 0$ is more weakly dependent on $\{\epsilon_i\}$, i.e. $\delta\Delta F^\ddagger/\delta\epsilon_i \cong \delta F(Q^\ddagger)/\delta\epsilon_i$, because $\delta F(Q_o \approx 0)/\delta\epsilon_i \cong 0$; less native structure is present in the unfolded state. The effect on the free energy of perturbations in $\{\epsilon_i\}$ is largest at intermediate Q ; there is no effect at the end points because at $Q = 0$ there are no native interactions, and at $Q = 1$ all native interactions are present and must add up to the total native stability E_N , which is fixed. In fact in the equations for the

free energy perturbation this effect is manifested by the factor of $Q(1 - Q)$ which multiplies every term, see e.g. eq.s (5.18), (5.23), and (5.32).

Because of the implicit functions mentioned above

$$\frac{\delta F}{\delta \epsilon_i} = \frac{\partial F}{\partial \epsilon_i} + \sum_j \frac{\partial F}{\partial Q_j} \frac{\partial Q_j}{\partial \epsilon_i} + \sum_j \frac{\partial F}{\partial Q_j} \frac{\partial Q_j}{\partial \mu} \frac{\partial \mu}{\partial \epsilon_i} \quad (5.5)$$

$$= \frac{\partial F}{\partial \epsilon_i} + \mu \sum_j \left[\frac{\partial Q_j}{\partial \epsilon_i} + \frac{\partial Q_j}{\partial \mu} \frac{\partial \mu}{\partial \epsilon_i} \right]. \quad (5.6)$$

However the term in square brackets is just the total derivative $\delta Q_j / \delta \epsilon_i$, so the sum vanishes because Q is a fixed parameter independent of ϵ_i [106]:

$$\sum_j \frac{\delta Q_j}{\delta \epsilon_i} = \frac{\delta}{\delta \epsilon_i} \sum_j Q_j = \frac{\delta}{\delta \epsilon_i} (MQ) = 0. \quad (5.7)$$

Differentiating eq. (4.8) immediately yields:

$$\frac{\partial \Delta F^\ddagger}{\partial \epsilon_i} \cong Q_i(Q^\ddagger), \quad (5.8)$$

so the perturbative change in the free energy barrier by varying a contact's energy is equal to the probability that contact was formed at Q^\ddagger (c.f. eq.s (3.2) and (3.19)).

This is strongly related to experimental ϕ_i values, which measure the change in the log rate after mutation over the change in difference in equilibrium populations of the folded and unfolded states [52, 107]. When the prefactor to the rate is unaffected by the mutation this is equivalent to the change with mutation in the barrier height over the change in the difference of the free energy minima [20, 52], which we refer to as ϕ' :

$$\phi'_i \equiv \frac{(\partial F^\ddagger / \partial \epsilon_i) - (\partial F_u / \partial \epsilon_i)}{(\partial F_f / \partial \epsilon_i) - (\partial F_u / \partial \epsilon_i)} = \frac{Q_i(Q^\ddagger) - Q_i(Q_U)}{Q_i(Q_F) - Q_i(Q_U)}. \quad (5.9)$$

When the nativeness in the unfolded state can be neglected, $Q_i(Q_U) \approx 0$, and when the native contacts in the folded state are essentially fully formed, $Q_i(Q_F) \approx 1$. Then eq. (5.9) becomes

$$\phi'_i \equiv \frac{\delta \Delta F^\ddagger}{\delta \epsilon_i} = \frac{\partial \Delta F^\ddagger}{\partial \epsilon_i} = Q_i(Q^\ddagger). \quad (5.10)$$

Equating ϕ values with contact probabilities assumes that contact probability be used as a kinetic reaction coordinate. In fact it has been observed in simulations that ϕ values correlate with Q_i values as well as any other reaction coordinate currently proposed [108].

Continuing now to find the energies ϵ_i^* which extremize the free energy, eq. (5.4) gives finally: $Q_i(Q^\ddagger, \mu^\ddagger = 0, \epsilon_i^*, \ell_i) = p$: the free energy is extremized when all the Q_i values are tuned to the same number at the barrier peak. This folding scenario is that of a symmetric funnel: the protein is equally likely to order from any place within it. Thus since $\sum_i Q_i = MQ$,

$$Q_i(Q^\ddagger, \mu^\ddagger = 0, \epsilon_i^*, \ell_i) = Q^\ddagger. \quad (5.11)$$

Solving eq. (5.11) for the energies using eq. (4.35) gives

$$\epsilon_i^* = T s_i + T \frac{d}{dQ} \left(\lambda [-Q \ln Q - (1 - Q) \ln(1 - Q)] \right)_{Q^\ddagger} - \frac{b^2}{2T}. \quad (5.12)$$

Subtracting $\bar{\epsilon}$ from ϵ_i by averaging eq. (5.12) yields:

$$\begin{aligned} \epsilon_i^* - \bar{\epsilon} &= T (s_i - \bar{s}) \\ &= -\frac{3}{2} T (\ln \ell_i - \overline{\ln \ell}) \end{aligned} \quad (5.13)$$

where eq. (4.20) was used. The free energy fluctuations $\delta f_i = 0$ in a uniform folding mechanism. Thus contacts pinching off longer loops ($\ell_i \gtrsim \bar{\ell}_i$) have lower (stronger) energies ($\epsilon_i < \bar{\epsilon}_i$) to make all the contact probabilities

equal at the barrier peak [109]. If correlations between contacts are fully accounted for, the Q_i values deviate slightly from Q away from the barrier peak, but the fluctuations away from uniform ordering are still strongly suppressed (see fig. 14C).

Evaluating the second derivative stability matrix in eq. (5.3) shows $Q_i = Q^\ddagger$ in eq. (5.11) to be an unstable maximum, as follows. From eq. (5.8)

$$\begin{aligned} \frac{\delta^2 F}{\delta \epsilon_j \delta \epsilon_i} &= \frac{\delta Q_i}{\delta \epsilon_j} = \frac{\partial Q_i}{\partial \epsilon_j} + \frac{\partial Q_i}{\partial \mu} \frac{\partial \mu}{\partial \epsilon_j} \\ &= -\frac{Q_i(1-Q_i)}{\lambda T} \left(\delta_{ij} + \frac{\partial \mu}{\partial \epsilon_j} \right) \end{aligned} \quad (5.14)$$

by eq. (4.35). Thus the second order change in the free energy at the extremum is

$$\sum_{i,j} \left(\frac{\delta^2 \Delta F^\ddagger}{\delta \epsilon_j \delta \epsilon_i} \right)_{\epsilon_i^*, \epsilon_j^*} \delta \epsilon_i \delta \epsilon_j = -\frac{Q^\ddagger(1-Q^\ddagger)}{\lambda T} \left[M \overline{\delta \epsilon^2} + \sum_{i,j} \left(\frac{\partial \mu}{\partial \epsilon_j} \right) \delta \epsilon_i \delta \epsilon_j \right]. \quad (5.15)$$

Since the perturbations $\delta \epsilon_i$ are independent, cross terms in the double sum of eq. (5.15) vanish, making the sum equal to

$$\sum_{i=1}^M \left(\frac{\partial \mu}{\partial \epsilon_i} \right) \delta \epsilon_i^2. \quad (5.16)$$

This term is negligible for the following reasons. First, note that $\partial F / \partial \epsilon_i = Q_i$ is $\sim \mathcal{O}(1)$. Then since $\partial \mu / \partial \epsilon_i = -(1/M)(\partial / \partial Q)(\partial F / \partial \epsilon_i)$ by eq. (4.36), the terms $\partial \mu / \partial \epsilon_i$ in eq. (5.16) are $\sim \mathcal{O}(1/M)$. So the sum of M terms in (5.16) is $\sim \mathcal{O}(1) \overline{\delta \epsilon^2}$, whereas the first term in eq. (5.15) is $\sim \mathcal{O}(M) \overline{\delta \epsilon^2}$ and dominates in the thermodynamic limit. Thus to order $\mathcal{O}(1/M)$:

$$\left(\frac{\delta^2 \Delta F^\ddagger}{\delta \epsilon_j \delta \epsilon_i} \right)_{\epsilon_i^*, \epsilon_j^*} = -\delta_{ij} \frac{Q^\ddagger(1-Q^\ddagger)}{\lambda^\ddagger T} \quad (5.17)$$

which is clearly negative, meaning that tuning the energies so that $Q_i = Q^\ddagger$ maximizes the free energy at the barrier peak. This is consistent with the intuitive arguments in section 3.3.B. Recall for example in section 3.3.B.3.B.4 we showed using thermodynamic perturbation theory that random perturbations to the contact energies always lowered the free energy barrier.

Substituting eq.s (5.8), (5.11), and (5.17) into (5.3) gives

$$\Delta F^\ddagger \{ \epsilon_i^* + \delta \epsilon_i \} \cong \Delta F_{\text{MF}}^\ddagger - M \frac{Q^\ddagger(1-Q^\ddagger)}{2\lambda^\ddagger T} \overline{\delta \epsilon^2}. \quad (5.18)$$

It should be noted this expression is very similar to eq. (3.5) obtained using a simple REM argument, and also to eq.s (3.17) and (3.23) using thermodynamic perturbation theory. The only major difference here is the factor of λ^\ddagger which accounts for the reduction in route entropy due to chain connectivity.

For an energetic standard deviation of about a $k_B T$ from the optimal distribution, the barrier goes down by about $\sim N k_B T / 2$ (we've let $M \approx 2N$, $\lambda^\ddagger \approx 1 - Q^\ddagger$ since the exponent α in (4.12) is about 1, and $Q^\ddagger \approx 1/2$). The barrier governed rate increases with native energetic heterogeneity as

$$k = k_o \exp \left(-\frac{\Delta F^\ddagger}{T} \right) = k_{\text{HOMO}} \exp \left(Q^\ddagger(1-Q^\ddagger) \frac{M \overline{\delta \epsilon^2}}{2\lambda^\ddagger T^2} \right) \quad (5.19)$$

which should be compared with eq. (3.6).

5.B. Including structural heterogeneity

The theory also allows us to investigate the effects of native structural variance on the barrier, as well as the correlations between structure and energetics. A perturbation analysis shows that structural variance lowers

the barrier as discussed in section 3.3.B.3, and that entropically likely contacts should be made stronger to lower the barrier, as discussed in section 3.3.A. In the model, entropically likely contacts are short-ranged. However they may occasionally be long-ranged when entropy is more precisely accounted for by accurately accounting for correlations between contacts (see figure 16).

Consider perturbing the free energy of a homogeneous system with $l_i = \bar{l}$, $\epsilon_i = \bar{\epsilon}$, $Q_i = Q^\ddagger$, by letting $l_i = \bar{l} + \delta l_i$ and $\epsilon_i = \bar{\epsilon} + \delta \epsilon_i$. Then,

$$\begin{aligned} \Delta F^\ddagger \{\bar{\epsilon} + \delta \epsilon_i, \bar{l} + \delta l_i\} &= \Delta F_{\text{MF}}^\ddagger \{\bar{\epsilon}, \bar{l}\} + \sum_i \left(\frac{\delta \Delta F^\ddagger}{\delta \epsilon_i} \right)_{\bar{\epsilon}, \bar{l}} \delta \epsilon_i + \sum_i \left(\frac{\delta \Delta F^\ddagger}{\delta l_i} \right)_{\bar{\epsilon}, \bar{l}} \delta l_i \\ &+ \frac{1}{2!} \sum_{i,j} \left(\frac{\delta^2 \Delta F^\ddagger}{\delta \epsilon_i \delta \epsilon_j} \right)_{\bar{\epsilon}, \bar{l}} \delta \epsilon_i \delta \epsilon_j + \frac{1}{2!} \sum_{i,j} \left(\frac{\delta^2 \Delta F^\ddagger}{\delta l_i \delta l_j} \right)_{\bar{\epsilon}, \bar{l}} \delta l_i \delta l_j + \frac{1}{2!} \sum_{i,j} \left(\frac{\delta^2 \Delta F^\ddagger}{\delta l_i \delta \epsilon_j} \right)_{\bar{\epsilon}, \bar{l}} \delta l_i \delta \epsilon_j \dots \end{aligned} \quad (5.20)$$

The first term in the expansion $\Delta F_{\text{MF}}^\ddagger \{\bar{\epsilon}, \bar{l}\}$ is the mean-field free energy eq. (4.31). The second term is zero at the extremum where $Q_i = Q^\ddagger$ by eq.s (5.8), (5.11) and (5.2), and the fourth term is given in eq. (5.18). The calculation of the third term proceeds along the same lines as the derivation of eq. (5.8). Like eq. (5.6), $\delta \Delta F / \delta l_i$ contains a term involving an explicit derivative of l_i , and implicit derivatives which are identically zero. The explicit term itself vanishes when evaluated for homogeneous fields. From eq. (4.32):

$$\left(\frac{\delta \Delta F^\ddagger}{\delta l_i} \right)_{\bar{\epsilon}, \bar{l}} = \frac{3}{2} T \left(\frac{Q_i - Q^\ddagger}{l_i} \right)_{\bar{\epsilon}, \bar{l}} = 0. \quad (5.21)$$

Calculation of the fifth term involves calculating $\delta Q_j / \delta l_i$, which proceeds analogously to the derivation of eq. (5.17) via (5.14):

$$\frac{\delta Q_j}{\delta l_i} \cong -\delta_{ij} \frac{3 Q_j (1 - Q_j)}{2 \lambda l_j} \quad (5.22)$$

which is again diagonal and negative as is eq. (5.17); raising the energy of a contact or increasing its loop length decreases that contact's probability of formation. From eq.s (5.21) and (5.22), the fifth and sixth terms in eq. (5.20) can be calculated, yielding

$$\begin{aligned} \Delta F^\ddagger \{\bar{\epsilon} + \delta \epsilon_i, \bar{l} + \delta l_i\} &= \Delta F^{\ddagger 0} \{\bar{\epsilon}, \bar{l}\} - M \frac{Q^\ddagger (1 - Q^\ddagger)}{2 \lambda^\ddagger T} \frac{1}{\delta \epsilon^2} \\ &- MT \frac{9 Q^\ddagger (1 - Q^\ddagger)}{8 \lambda^\ddagger} \frac{\delta l^2}{\bar{l}^2} - M \frac{3 Q^\ddagger (1 - Q^\ddagger)}{4 \lambda^\ddagger} \frac{\delta l \delta \epsilon}{\bar{l}} \end{aligned} \quad (5.23)$$

The third term in eq. (5.23) indicates that structural dispersion also lowers the barrier, in agreement with the arguments given in sect. 3.3.B.3. The fourth term indicates that the free energy barrier is additionally lowered in the model when shorter range contacts become stronger energetically ($\delta l_i < 0$ and $\delta \epsilon_i < 0$) or longer range contacts become weaker energetically ($\delta l_i > 0$ and $\delta \epsilon_i > 0$). This means in general that the free energy is additionally lowered when fluctuations are correlated so as to further increase the variance in contact participations, in agreement with the intuitive arguments given in section 3.3.A. Note again that all reductions in free energy due to structural and/or energetic heterogeneity scale extensively with system size.

5.C. Illustrations using a lattice model protein and functional theory

We illustrate in figures 9–15 the general effects of introducing heterogeneity to a model system. Results are shown for a G \bar{o} protein, modeled with the free energy functional theory using reasonable parameters and loop-length distribution given in table I, and also simulated on a lattice (see also reference [43] for a concise treatment of some of these phenomena). The lattice protein is a chain of 27 monomers constrained to reside on vertices of a three-dimensional cubic lattice (see fig. 1). Details of the model and its behavior can be found in ref.s [25, 110–113]. Monomers have non-bonded contact interactions with a G \bar{o} potential (native interactions only). Corner, crankshaft, and end moves are allowed. Free energies and contact probabilities are obtained by equilibrium Monte Carlo sampling using the histogram method [111]. Sampling error is < 5%. Coupling energies were chosen by first running a simulated annealing algorithm to find the set of native energies $\{\epsilon_i^*\}$

that makes all the contact probabilities equal at the barrier peak: $Q_i(\{\epsilon_i^*\}) = Q^\ddagger$ (c.f. table I for the energies which induce uniform folding for the native structure in fig. 1). Energies are always constrained to sum to a fixed total native energy: $\sum_i \epsilon_i = M\bar{\epsilon}$, i.e. overall stability is fixed. Energies are relaxed from $\{\epsilon_i^*\}$ by letting

$$\epsilon_i = \epsilon_i^* + \alpha(\bar{\epsilon} - \epsilon_i^*). \quad (5.24)$$

For the simulation results, the values $\alpha = 0, 1, 1.35, 2.05$ were used in the figures, and for the theoretical results, the values $\alpha = 0, 0.5, 0.65, 1.9$ are used. When $\alpha = 0$, $\{\epsilon_i\} = \{\epsilon_i^*\}$ and all the contact probabilities are the same at the barrier peak; the folding barrier is maximized. When $\alpha = 1$, all the energies are equal ($\{\epsilon_i\} = \{\bar{\epsilon}\}$); the entropy at the barrier peak is maximized. When $\alpha \approx 1.35$ ($\alpha \approx 0.65$ in the theory) the free energy barrier vanishes, and when $\alpha \approx 2.05$ ($\alpha \approx 1.9$ in the theory), folding occurs by only a few routes—essentially one route through the transition state. The discrepancy between the theory and the simulation for the values of α required to produce a given folding mechanism is most likely because the theory for loop closure, eq.s (4.19) and (4.20) overestimates the dispersion in entropy losses for contact formation.

In the figures to follow we compare thermodynamic quantities and folding mechanisms for various energy functions, consistently using the following convention; thin solid: $\alpha_{\text{SIM}} = 0, \alpha_{\text{THRY}} = 0$; thick solid: $\alpha_{\text{SIM}} = 1.0, \alpha_{\text{THRY}} = 0.5$; long dashed: $\alpha_{\text{SIM}} = 1.35, \alpha_{\text{THRY}} = 0.65$; short dashed: $\alpha_{\text{SIM}} = 2.05, \alpha_{\text{THRY}} = 1.9$.

5.C.1. Total Energy

Figure 9 shows a plot of the total energy as a function of Q obtained from lattice simulations of a Gō model to the structure shown in fig. 1. When native energies are uniform, the total energy decreases linearly with Q , since the total energy (eq. (4.5) with $b = 0$) is $\sum_i Q_i \epsilon_i = \bar{\epsilon} \sum_i Q_i = E_N Q$. When energies are tuned so that contact probabilities at the barrier peak are all equal ($Q_i(\epsilon_i^*, Q^\ddagger) = Q^\ddagger$, see eq. (5.11)), the total energy at the barrier peak position is equal to the total energy when $\epsilon_i = \bar{\epsilon}$, since $\sum_i Q_i(Q^\ddagger) \epsilon_i = Q^\ddagger \sum_i \epsilon_i$ which again equals $E_N Q^\ddagger$. So as the coupling energies are relaxed from $\{\epsilon_i^*\}$ to $\{\bar{\epsilon}\}$ in eq. (5.24), the energy at the barrier peak hardly changes, as can be seen from the figure (shifting of the peak position is a small effect). Further perturbing the coupling energies results in an overall decrease in total energy. Temperatures are adjusted to T_F for all curves in fig. 9, however T_F is roughly constant for the upper 3 curves (see fig.s 12 and 19); for the case when the energies are tuned to induce route-like folding: $\{\epsilon_i\} = \{\epsilon_i^R\}$, the folding temperature is about a factor of 6 lower. While heterogeneity effects on the total energy in fig. 9 and entropy in fig. 10 below may appear fairly small, the effect on the barrier and corresponding rate may be large, since the barrier arises from the cancellation of these two large terms, and the rate is proportional to the exponential of this difference.

5.C.2. Total Entropy

Figure 10 shows a plot of the total entropy as a function of Q from simulations of the Gō model mentioned above. When the native energies are all the same, $\{\epsilon_i\} = \{\bar{\epsilon}\}$ (maximal solid curve in fig. 10), the entropy is larger than for any other distribution as shown in section 3.3.C. We derive this result now using the free energy functional theory.

First, the total entropy at Q depends on the relative occupation probabilities and so does not depend explicitly on the total energy. One can see this by taking the derivative:

$$\frac{\partial S}{\partial E_N} = \frac{\partial S}{\partial (\sum_i \epsilon_i)} = \frac{1}{M} \sum_i \frac{\partial S}{\partial \epsilon_i} = 0 \quad (5.25)$$

since the entropy does not depend explicitly on the coupling energies ($\partial S / \partial \epsilon_i = 0$). The last equation follows from the properties of the directional derivative (c.f. Appendix A). This independence of canonical entropy on total energy is analogous to the property that the Lagrangian for a system of particles not under any external forces is independent of the center of mass coordinate. One can solve Newton's equations without the constraint and obtain a zero frequency normal mode corresponding to the whole system in uniform motion. Keeping the constraint introduces a new equation and unknown (the Lagrange multiplier), and solving the eigenvalue problem yields that the multiplier is zero. Another example is a thermal bath of photons, which has no constraint on the total number of photons. Thus the Lagrange multiplier for this constraint—the chemical potential, is zero. The Lagrange constraint here appears in the form $p \sum_i \epsilon_i$ as in eq. (5.4), which has the form

of a Legendre transform with the Lagrange multiplier p being proportional to $\partial S/\partial E_N$, just as the Lagrange multiplier μ in eq. (4.36) is proportional to $\partial F/\partial(MQ)$. So the multiplier p is identically zero.

We take the extremum of the entropy, now explicitly introducing the constraint that Q is fixed:

$$\delta \left[S + \nu \sum_j Q_j \right] = \sum_i \left[\frac{\delta S}{\delta \epsilon_i} + \nu \frac{\delta Q_j}{\delta \epsilon_i} \right] \delta \epsilon_i = 0 \quad (5.26)$$

for arbitrary and independent variations $\delta \epsilon_i$. Since the entropy does not depend explicitly on ϵ_i ,

$$\frac{\delta S}{\delta \epsilon_i} = \sum_j \frac{\partial S}{\partial Q_j} \frac{\delta Q_j}{\delta \epsilon_i}. \quad (5.27)$$

Using $S = (E - F)/T$, and eq.s (4.5) and (4.34),

$$\frac{\partial S}{\partial Q_j} = \frac{\epsilon_j}{T} + \frac{\mu}{T}. \quad (5.28)$$

Now by the properties of the Legendre transform,

$$\nu = -\frac{1}{M} \frac{\partial S}{\partial Q} \quad (5.29)$$

see the analogous eq. (A.3). Again using $S = (E - F)/T$, eq. (A.3), and the directional derivative on E (c.f. eq.(A.5)), we obtain

$$\nu = -\frac{\bar{\epsilon}}{T} - \frac{\mu}{T}. \quad (5.30)$$

Putting eq.s (5.28) and (5.30) into eq. (5.26) gives

$$\sum_j \left[\frac{\epsilon_j - \bar{\epsilon}}{T} \right] \frac{\delta Q_j}{\delta \epsilon_i} = 0 \quad (5.31)$$

and using eq.(5.14), i.e.

$$\frac{\delta Q_j}{\delta \epsilon_i} = -\delta_{ij} \frac{Q_j(1 - Q_j)}{\lambda T} \quad (5.32)$$

eq. (5.31) becomes

$$(\epsilon_i - \bar{\epsilon}) \frac{Q_i(1 - Q_i)}{\lambda T} = 0, \quad (5.33)$$

whose only solution is $\epsilon_i = \bar{\epsilon}$, i.e. all the coupling energies are equal. Taking the second derivative yields

$$\left(\frac{\delta^2 S}{\delta \epsilon_j \delta \epsilon_i} \right)_{\epsilon_i = \bar{\epsilon}, \epsilon_j = \bar{\epsilon}} = -\delta_{ij} \frac{Q_i(1 - Q_i)}{\lambda T} \quad (5.34)$$

which is negative indicating the extremum is a maximum. Thus the thermal entropy is maximized for uniform coupling energies, for proteins well-designed enough to be modeled by Gō-like models.

Keeping the Lagrange constraint $\sum_i \epsilon_i = E_N$ modifies eq. (5.33) to

$$\begin{aligned} \delta \epsilon_i \alpha_i + p &= 0 & 1 < i < M \\ \sum_i \delta \epsilon_i &= 0 \end{aligned} \quad (5.35)$$

where $\alpha_i \equiv Q_i(1 - Q_i)/\lambda T$ and p is the undetermined multiplier. Equations (5.35) constitute $M + 1$ equations for $M + 1$ unknowns (the $\delta \epsilon_i$ and p). The solution then amounts to finding the determinant of the matrix

$$\text{Det} \begin{bmatrix} \alpha_1 & 0 & \dots & 0 & 1 \\ 0 & \alpha_2 & \dots & 0 & 1 \\ \vdots & \vdots & \ddots & \vdots & \vdots \\ 0 & 0 & \dots & \alpha_M & 1 \\ 1 & 1 & \dots & 1 & 0 \end{bmatrix} = 0 \quad (5.36)$$

which is readily evaluated, and consists of M negative terms, which are all possible ways to pick $M - 1$ of the M α_i 's, e.g. if $M = 4$, the determinant is $-\alpha_1\alpha_2\alpha_3 - \alpha_1\alpha_2\alpha_4 - \alpha_1\alpha_3\alpha_4 - \alpha_2\alpha_3\alpha_4$. Thus the determinant is never zero, so there is no solution other than the trivial solution, where all $\delta\epsilon_i = 0$, which is again the condition that $\epsilon_i = \bar{\epsilon}$. Putting this condition in eq.s (5.35), we again recover that the Lagrange constraint $p = 0$.

5.C.3. Free Energy

Figure 11 shows the total free energy $F(Q)$ in units of $\bar{\epsilon}$ for the simulations and functional theory, for various energy functions. For the simulations $F(Q)$ is obtained from $E(Q) - T_F(\{\epsilon_i\})S(Q)$ where $E(Q)$ is shown in fig. (9) and $S(Q)$ shown in fig. (10). The transition temperature $T_F(\{\epsilon_i\})$ is defined as the temperature giving a native ($Q = 1$) occupation probability of 50% (see fig. 12). For the theory $F(Q)$ is obtained from eq.s (4.30), (4.31), and (4.32), and the transition temperature T_F is defined as the temperature where the probability for $Q > 0.9$ is 50% (the transition temperature is not strongly dependent on this cutoff). For ϵ_i^* (thin solid curve) the folding barrier is maximized, see eq. (5.17). Here the profile is largely a function only of the mean loop length $\bar{\ell}$ and system size N (see eq. (4.31)), since most structural features are tuned away by adjusting the native energies. The only other residual structural features which remain are the effects of native structure on the exponent α in the route entropy reduction, eq. (4.11), which is probably a small effect compared to the effects we consider here. For uniform native energies, the transition state energy hardly changes as explained in section 5.5.C.1, but the entropy increases to its maximal value as explained in section 5.5.C.2. So the barrier height initially decreases for entropic reasons (see also fig.s 12 and 17). For the lattice model the barrier is reduced by about a factor of 2, (thick solid in upper plot) and for the theory the barrier disappears entirely at the transition temperature, the curve residing between the long-dashed and short-dashed curves in the lower plot. The thick solid curve in the theory plot is for about half the energetic dispersion required to tune the system to homogeneous folding; this results in the same reduction in folding temperature as the simulations. Further perturbing the energies to $\{\epsilon_i^o\}$ eliminates the barrier entirely at the transition temperature making the transition second order (long dashed curves). For the simulations, between $\{\bar{\epsilon}\}$ and $\{\epsilon_i^o\}$ the barrier decreases because the energy at the transition state lowers while the entropy doesn't change to first order. In the theory there is sufficient entropic variance to kill the barrier before relaxing all energies to a uniform distribution $\{\bar{\epsilon}\}$, however $\{\epsilon_i\}$ for the long dashed line in the theory has a relative variance $\delta\epsilon/\bar{\epsilon}$ of only about 0.15 compared to about 0.47 for the maximum barrier. Cooperative effects [34, 60–62] or entropic reduction arising from the coupling of chain stiffness with folding [114] restores a barrier for uniform native energies. As energies are further perturbed to a distribution $\{\epsilon_i^R\}$ causing folding to occur by a single dominant route (short dashed), folding becomes strongly downhill at the the transition temperature, which drops sharply by about a factor of 6. For a system with non-native as well as native interactions, the free energy would be less downhill and much more rugged at these temperatures. Folding would be exceedingly slow because the protein would spend a long time in individual traps.

Figure 12 shows the total barrier height ΔF^\ddagger , in units of the mean native contact strength $\bar{\epsilon}$, vs. the RMS native energetic variance in the same units. Plotted are results from simulation of a lattice 27-mer G \bar{o} model; the analytic theory gives qualitatively the same results (see fig. 17). Native interactions $\{\epsilon_i\}$ are tuned to a distribution $\{\epsilon_i^*\}$ that symmetrizes the funnel to uniform ordering at the barrier peak, giving the largest barrier at the upper right of the figure (see eq. 5.17). The energies here are anticorrelated with their loop lengths in that more negative energies are required for the longer loops to have equal free energies (see eq. 5.13). A large dispersion in interaction strengths is required to achieve this scenario, which may be impossible to achieve in practice (see table I). Interactions are then uniformly relaxed via eq. (5.24) to $\{\epsilon_i\} = \{\bar{\epsilon}\}$ (i.e. $\delta\epsilon_i = 0$) and the barrier is reduced by a factor of 2, due to entropic gains in the transition state ensemble (TSE) (see eq. (5.34)). The ϵ_i are then continued to evolve - now $\delta\epsilon_i$ begins to correlate with loop length and anti-correlate with contact probability (c.f. eq. 5.24), which further increases the heterogeneity. The barrier decreases now because energetic gains win over entropic losses in the TSE, and eventually the barrier vanishes at coupling energies $\{\epsilon_i^o\}$. We should emphasize here that $\{\epsilon_i^o\}$ is not unique; many sufficiently heterogeneous

distributions of native stability may kill the barrier. All the while the folding temperature T_F (dashed curve) defined here as the temperature where the native state at $Q = 1$ is 50% occupied, decreases by only 10% and remains well above the putative estimate of the glass temperature $T_G \cong T_F/1.6$ (thin horizontal dot-dashed line at lower right). The fact that T_F/T_G was roughly constant as native interactions were varied indicates that the prefactor to the folding rate, k_o in eq. (1.3) is roughly constant (see sect. 5.5.F). Folding rates are governed largely by the free energy barrier in this regime (see fig. 18 below) and can be treated with thermodynamic analysis. Because the entropy of the bottleneck is not constant as $\delta\epsilon/\bar{\epsilon}$ is varied, another valid measure of T_F/T_G for this system is T_F times the root entropy per residue at the bottleneck (thin solid line with squares). This measure actually shows a slightly increasing trend as $\epsilon_i \rightarrow \bar{\epsilon}$ and only slight decrease as $\{\bar{\epsilon}\} \rightarrow \{\epsilon_i^o\}$.

5.D. Folding Mechanisms: Route Entropy, Halo Entropy, and Contact Probability

We continue by investigating different possible folding mechanisms to the same structure, induced by different distributions of native stability. So far we have seen that in Gō-like models of well-designed proteins, governed by an energy function with pair interactions, the folding mechanism to a given structure may involve a barrier of various heights (fig. 11) while the total entropy and energy are relatively unaffected (figs. 9 and 10), depending on how native interactions are distributed throughout the protein. The barrier is sensitive to perturbations because it arises from the cancellation of large terms: the total entropy and energy [61, 105]. We have seen so far that it is quite difficult to tune away all the effects of native topology, or induce folding through one or a few routes. Now we investigate some of the properties of partially native states when folding occurs by various mechanisms. We again vary the distribution of native energies by varying values of α in eq. (5.24).

Figure 13 shows the route entropy $\mathcal{S}_{\text{ROUTE}}$ over the number of contacts M as a function of Q , for the 27-mer lattice model (Top) and for the functional theory (Bottom). In both cases eq. (4.11) is used to calculate the mixing entropy from the contact probabilities $\{Q_i\}$. For native contact distribution $\{\epsilon_i^*\}$ which induces homogeneous folding through the barrier peak (thin solid), the curve essentially reproduces that in fig. 7. This distribution maximizes the route entropy. For a uniform distribution of native energies (Top figure, thick solid) there is a reduction from the homogeneously ordering case solely due to the topology of the native structure. Different native structures will have different characteristic curves. For the theory curves, the same native energy distributions used above in fig. 11 are used here. For interactions $\{\epsilon_i^o\}$ which kill the barrier, the route entropy is further reduced (long dashed). The upper 3 curves in both plots are funneled folding mechanisms with barrier heights varying from their maximum to zero. The bottom curves (short dashed) are route entropies for a folding mechanism involving a small number of routes. If $\mathcal{S}_{\text{ROUTE}} = 0$, only one route to the native state is allowed, because then all contact probabilities Q_i are only zero or one at any degree of nativeness, and if this is the case each successive bond made in folding must always be the same one at each and every degree of nativeness. It is interesting that in both theory and simulation there are fluctuations in the route entropy. These correspond to the necessary fractional values of contact formation probability present when a particular contact begins to be formed, as long as contact probabilities Q_i go from zero to one over a finite width ΔQ (see fig. 14).

Figure 14 shows the contact formation probability $Q_i(Q)$ as a function of Q for all contacts. The top row is the lattice simulation result, the bottom row from the analytical theory, eq. (4.35). The left column is for a route-like folding scenario, the right column for a uniform folding scenario at the barrier peak. Energies are chosen from eq. (5.24) with values for α shown above each figure. There are less curves in the analytic theory because contacts with the same loop length (which have the same energy) have the same $Q_i(Q)$. In the route-like folding scenario, contacts remain unformed until their free energy of contact formation $f_i = \epsilon_i - Ts_i(Q)$ equals $-\mu(Q) = (1/M)\partial F/\partial Q$, for larger Q they are then essentially formed (see eq. (4.35) with $s_{\text{ROUTE}}^o = 0$ and $b = 0$). Here $\mu(Q)$ in eq. (4.35) serves as a chemical potential for each contact. Fluctuations in route entropy for a route-like folding scenario can be understood through the behavior of contact formation probabilities. For this folding mechanism contact probabilities are approximately either zero or one. But as Q increases, new contacts must be formed and so their formation probabilities must go from zero to one, over some finite interval ΔQ for any finite sized system with a reasonable distribution of native energies. In this range ΔQ , the contact(s) increasing from zero to one have fractional occupation probabilities and so contribute to the route entropy, causing the bumps seen in figure 13. In the uniform folding scenario, all $Q_i(Q^\dagger) \approx Q^\dagger$ at the barrier peak position. They deviate away from Q away from the barrier peak in the lattice model because of the nontrivial dependence of the loop entropy on nativeness. Deviations away from Q in the theory are due to the cut-off introduced into the entropy function mentioned above, so that eq. (5.13) is not strictly valid.

When contact probability is governed by native topology, as in figure 2, the variance in Q_i values is in between the two extreme cases shown here in figure 14.

We can make a connection with earlier polymer theory by investigating the total entropy minus the route entropy $\mathcal{S}_{\text{FLORY}} \equiv Ns_o + \mathcal{S}_{\text{BOND}}$ (see fig. 15). This can be thought of as the residual entropy of the effective halo dressing the partially native structures, and is analogous to the polymer entropy in a cross-linked system studied by Flory and others [100, 115, 116]. As mentioned in the comments after eq. (4.29), fluctuations away from uniform folding raise the bond entropy and thus the Flory entropy, as can be seen in figure 15 for both simulations and theory. For the uniform folding scenario, there is a value of $Q_v < 1$ where the Flory entropy runs out (see again comments after eq. (4.29)). In a uniform folding scenario above Q_v , all residual entropy is combinatoric- if MQ_v crosslinks were permanently made with equal probability anywhere in the protein, there would be no entropy left in the system. The mean-field prediction gives $Q_v \approx 2s_o/3z \approx 0.87$. The lattice value of $Q_v \approx 0.65$ is considerably lower probably because ideal chain statistics used in the theory overestimates the entropy actually present in a partially constrained lattice polymer of length $N = 27$. The folding mechanism having few routes has essentially the largest Flory entropy here because following the recipe of eq. (5.24) weights a native core with naturally large halo entropy. Weighting other cores would in general not give the same result.

We continue the comparison between theory and simulation by plotting several quantities in figure 16, for a folding mechanism with intermediate barrier height ($\alpha_{\text{SIM}} = 1.0$, $\alpha_{\text{THRY}} = 0.5$ in eq. (5.24)), and for energies ϵ_i^* which induce a uniform folding mechanism in fig. 16C. Plot 16A shows the correlation between theory and simulation of contact probability at the barrier peak $Q_i(Q^\ddagger)$ given in the theory by eq. (4.35). Contacts with the same loop length have the same Q_i value in the theory but not in the simulation (due to entropic differences even for contacts having the same loop length). However the average of the simulational contact probabilities (squares in fig. 16A) correlates well with the theory (correlation coefficient = 0.93), indicating that the theory captures the average trend, but there are potentially important many-body effects in the calculation of the entropy loss upon contact formation. Figure 16B shows the trend in contact probability with increasing loop length, by replotting the theory and data against log loop length. The solid line is the theoretical result of eq. (4.35) with eq.s (4.19) and (4.20). Again the data fluctuate significantly about this curve, but the theory captures the trend in the average values (squares) (as before, correlation coefficient 0.93). Figure 16C shows the results of tuning the energies to induce uniform folding, for theory and simulation. The solid line is the result of equation (5.13): $\delta\epsilon_i = T_F\delta s_i$. The data points with error bars are the values extracted from lattice simulations. Again the theory captures the overall trend (correlation coefficient 0.71), but there are still significant fluctuations about the average.

5.E. Measures of routing

Since the free energy barrier is maximized for a uniform funnel folding mechanism (eq. 5.17), we expect the barrier height to be decreasing function of the dispersion in Q_i values at the barrier peak $\overline{\delta Q^2}(Q^\ddagger) = \langle (Q_i - Q^\ddagger)^2 \rangle$. Let us introduce a measure of ‘‘routing’’ $\mathcal{R}(Q^\ddagger)$ through the bottleneck by the function

$$\mathcal{R}(Q) = \frac{\langle \delta Q^2 \rangle}{\langle \delta Q^2 \rangle_{\text{MAX}}} = \frac{\langle \delta Q^2 \rangle}{Q(1-Q)}. \quad (5.37)$$

The denominator is the most route-like the system can get at Q , i.e. if MQ contacts were made with probability 1 and $M - MQ$ contacts were made with probability 0, then $\langle (Q_i - Q)^2 \rangle = (1/M)(MQ(1-Q))^2 + (M - MQ)Q^2 = Q(1-Q)$. Thus $\mathcal{R}(Q)$ is between 0 and 1. $\mathcal{R}(Q)$ is proportional to the lowest order correction to the route entropy (4.11) when fluctuations δQ are present:

$$\mathcal{S}_{\text{ROUTE}}(\{Q + \delta Q_i\}) \cong \mathcal{S}_{\text{ROUTE}}^o - \frac{M\lambda}{2}\mathcal{R}(Q). \quad (5.38)$$

In the (non-perturbative) limit $\mathcal{R}(Q) = 1$, $\mathcal{S}_{\text{ROUTE}} = 0$ and only one route to the native state is allowed, i.e. since all Q_i are only zero or one at any degree of nativeness, each successive bond added at that degree of nativeness must always be the same one.

Using eq. (5.32) we can relate the fluctuations in optimal energies $\delta\epsilon_i$ in terms of fluctuations from the uniform contact probabilities δQ_i as $\delta\epsilon_i = -\lambda T \delta Q_i / Q^\ddagger(1 - Q^\ddagger)$, and then substitute this along with (5.17) into eq. (5.3) to obtain the decrease in barrier height with route measure:

$$\delta\Delta F^\ddagger \cong -M \frac{\lambda^\ddagger T}{2} \frac{\overline{\delta Q^2}}{Q^\ddagger(1-Q^\ddagger)} = -M \frac{\lambda^\ddagger T}{2} \mathcal{R}(Q^\ddagger). \quad (5.39)$$

As noted above (see e.g. comments after eq. 5.23), the reduction in the barrier height due to ordering heterogeneity scales extensively with system size. A dispersion in contact participations $\overline{\delta Q^2} = 0.05$ which is about 20% of the maximal dispersion ($\approx 1/4$, taking $Q^\ddagger \approx 1/2$) lowers the barrier by about $0.1Nk_B T$ or about $5k_B T$ for a chain of length $N \approx 50$, believed to model a protein with $\approx 100aa$ [27]. We should note here that renormalizing real amino acids into coarse-grained monomers may underestimate the heterogeneity effect, because small-scale free energy fluctuations do not average out upon coarse-graining, but will still add up extensively. Plots of the route measure as a function of Q for the various possible folding scenarios were given in reference [43]; essentially the same information is contained in the route entropy plotted here in figure 13.

Figure 17 shows the barrier height at the transition temperature T_F in units of $\bar{\epsilon}$, vs. the route measure at the barrier peak $\mathcal{R}(Q^\ddagger)$ (T_F is itself weakly dependent on $\mathcal{R}(Q^\ddagger)$; see e.g. fig. 12). There is a monotonically decreasing trend for both theory and simulation. The solid line in figure 17 is the theoretical result for a model with parameters in table I. The barrier vanishes for roughly the same magnitude of route measure in both theory and simulation, even though different dispersions in contact energies are required to produce these route measures. We can examine the effects of heterogeneity on a uniform, idealized funnel, where all loops have length $\ell_i = \bar{\ell} \approx 9$, the average of the lattice model native structure of figure 1; and initially all energies $\epsilon_i = \bar{\epsilon}$ (long dashed line in fig. 17). Here too breaking the ordering symmetry $Q \rightarrow \{Q_i\}$ by random perturbations on ϵ_i lowers the thermodynamic barrier, as explained in sections 2.2.A and 3.3.B; the barrier goes down because the energy decreases more than the route-entropy decreases. Perturbing the structure by including entropic dispersion via $\delta\ell_i$ yields a similar result (c.f. eq. (5.23)). The short dashed line in figure 17 is the perturbation result for this model from eq. (5.39), which agrees well with the full non-perturbative result for small \mathcal{R} .

5.F. Kinetics of folding times

We can verify that the heterogeneity effect on the barrier translates directly to an increase in folding rate by simulating long Monte Carlo runs and measuring the distribution of folding times at the transition temperature T_F for various energy functions $\{\epsilon_i\}$ (see fig. 18).

To estimate the increase in rate assuming the prefactor is not important, take the barrier heights from fig. 17 and neglect the change in transition temperature T_F since it only depends weakly on \mathcal{R} (see fig. 12). Then the ratio of folding times, say at $\mathcal{R} = 0$ and $\mathcal{R} = 0.2$, is

$$\frac{\tau_F(\mathcal{R} = 0)}{\tau_F(\mathcal{R} = 0.2)} = \frac{\exp(\Delta F^\ddagger(\mathcal{R} = 0)/T_F)}{\exp(\Delta F^\ddagger(\mathcal{R} = 0.2)/T_F)} \approx \frac{\exp(2.1/0.7)}{\exp(1.2/0.7)} \approx 3.6 \quad (5.40)$$

which is in reasonable agreement with the measured ratio of about 3 (see fig. 18). For the heterogeneous Gō models considered here, the folding time is well approximated by an Arrhenius law with constant prefactor, indicating that the time scale in the reconfigurational kinetics is not strongly influenced by the degree of routing, at least up until the barrier vanishes.

We can expand equation (1.3) to first order in changes in the barrier height δF^\ddagger , folding temperature δT_F , and prefactor δk_o to obtain a condition that must be satisfied for the rate to increase under perturbations of native energy:

$$\begin{aligned} \frac{\delta F^\ddagger}{T_F} &\lesssim \frac{\delta k_o}{k_o} + \frac{F^\ddagger \delta T_F}{T_F^2} \\ &\lesssim \left(\frac{\partial \ln k_o}{\partial T} + \frac{F^\ddagger}{T_F^2} \right) \delta T_F, \end{aligned} \quad (5.41)$$

where we have made the approximation in the second inequality that the prefactor is most strongly affected by changes in the folding temperature, since the closer T_F is to T_G the slower reconfigurational dynamics is within the protein, and we have seen in fig. 18 that the prefactor is nearly independent of the native energy distribution; then $\delta k_o \approx (\partial k_o / \partial T) \delta T$. For well-designed folders, the folding transition temperature T_F is above the dynamic glass temperature of the system, and reconfigurational dynamics is largely unactivated [117, 118], i.e. escape from individual traps does not dominate the kinetics. In this regime, the prefactor, which is related

to the hopping time, is nearly temperature independent: $\partial \ln k_o / \partial T \ll F^\ddagger / T^2$. Then the condition given in eq. (5.41) becomes

$$\frac{\delta F^\ddagger}{F^\ddagger} \lesssim \frac{\delta T_F}{T_F} \quad (5.42)$$

For slower folders, effects on the prefactor may be as important as effects on the barrier, however for the well-designed folders considered here the rate increases so long as the relative barrier height decreases more strongly than the relative change in folding temperature. This is seen to be the case in figure 19.

5.G. Mean loop length dependence of the barrier height

Experimental evidence has shown a strong correlation of folding rate with a quantity in our model equal to the mean loop length divided by the total chain length [30]. Since no strong correlation with N is observed at least for typical protein sizes, we are interested in testing if the barrier height in our model correlates with $\bar{\ell}$, at fixed N .

We seek the change in free energy δF upon a change in the quantity $(1/M) \sum_i \ell_i$. This can be found by utilizing the directional derivative (see Appendix A and eq. A.5):

$$\frac{\delta F}{\delta \bar{\ell}} = M \frac{\delta F}{\delta (\sum_i \ell_i)} = \left(\sum_i \hat{i} \right) \cdot \left(\sum_j \frac{\delta F}{\delta \ell_j} \hat{j} \right) = \sum_i \frac{\delta F}{\delta \ell_i}. \quad (5.43)$$

Using again the analog of eq. (5.6) that we used already to obtain eq. (5.21), the total derivative of F with respect to ℓ_i is equivalent to the partial derivative. The free energy F depends on ℓ_i explicitly only through the bond entropy eq. (4.26), which is composed of a mean-field term depending on the sum $\bar{\ell}$ plus a fluctuation term, eq.s (4.27) and (4.28). Noting that

$$\frac{\partial \mathcal{S}_{\text{MF}}(Q, \bar{\ell})}{\partial \ell_i} = \frac{1}{M} \frac{\partial \mathcal{S}_{\text{MF}}(Q, \bar{\ell})}{\partial \bar{\ell}}$$

we obtain

$$\frac{\partial F}{\partial \bar{\ell}} = -T \frac{\partial \mathcal{S}_{\text{BOND}}}{\partial \bar{\ell}} = \frac{3}{2} \frac{MT}{(\bar{\ell} - 1)^2} [\ln(1 + (\bar{\ell} - 1)Q) - Q \ln \bar{\ell}] + \frac{3}{2} MT \left\langle \frac{\delta Q}{\bar{\ell}} \right\rangle. \quad (5.44)$$

The first term in expression (5.44) is always positive for $Q > 0$. The second term weights loops with smaller ℓ_i more heavily, and for these loops $\delta Q > 0$, so the second term is always positive when entropic effects are considered alone. The native energies would have to be specially tuned to change the sign of this term. Moreover the whole expression is zero when $Q = 0$, so we conclude that the effect of increasing the mean loop length is to increase the barrier height ΔF^\ddagger . This effect is illustrated in fig. 20 for the simple case where $\ell_i = \bar{\ell}$, where the second term in (5.44) is zero; this is a lower limit to the actual increase in barrier.

As eq. (5.44) implies, the change in barrier height with mean loop length is an entropic effect; proteins with native structures having larger mean loop length have lower entropy near the transition state. Another perhaps simpler way to see this is to note that the entropy of loop closure must become larger (more negative) as the loop length for that contact is increased. From eq.s (4.19) and (4.20) and setting $\ell_i = \bar{\ell}$ for purposes of illustration,

$$\frac{\partial s_i}{\partial \bar{\ell}} \approx -\frac{1 - Q}{\bar{\ell}(1 + (\bar{\ell} - 1)Q)} < 0. \quad (5.45)$$

Therefore more entropy is lost in contact formation for structures with larger mean loop length. Furthermore since

$$\frac{\partial^2 s_i}{\partial Q \partial \bar{\ell}} \approx \frac{1}{(1 + (\bar{\ell} - 1)Q)^2} > 0, \quad (5.46)$$

this effect is largest at low degrees of nativeness (e.g. from eq. (5.45) at $Q = 0$, $\partial s_i / \partial \bar{\ell} \approx -1/\bar{\ell}$ while at $Q = 1$ $\partial s_i / \partial \bar{\ell} \approx 0$): the entropy becomes more of a convex down function as $\bar{\ell}$ is increased, see fig. 21. Since the free energy barrier arises from the incomplete cancellation of entropy and energy (which is independent of $\bar{\ell}$) as Q increases, a more convex down entropy indicates a larger barrier height.

5.H. Dependence of barrier heights and rates on structural variance

By eq. (5.23), if we let $\epsilon_i = \bar{\epsilon}$ and fix $\bar{\ell}$, the folding barrier is lower for structures with larger variance in loop energies $\overline{\delta\ell^2}$. For proteins sufficiently well-designed that the folding rate k_F near the transition temperature is governed by the free energy barrier as in eq. (1.3), then

$$\ln \frac{k_F(\overline{\delta\ell^2})}{k_F(0)} \approx MQ^\ddagger \frac{\overline{\delta\ell^2}}{\bar{\ell}^2} \quad (5.47)$$

where we have also neglected changes in the folding transition temperature, since accounting for this is a higher order effect. We have also let $\lambda^\ddagger \approx 1 - Q^\ddagger$ since α in eq. (4.12) is approximately one (see table I). Most importantly the perturbation result neglects changes in the unfolded free energy on structural variance, as well as changes in the amount of native structure in the unfolded state. These reduce the trend on the rate due to structural variance. In general we should use

$$\ln \frac{k_F(\overline{\delta\ell^2})}{k_F(0)} \cong \frac{\Delta F^\ddagger(0)}{T_F(0)} - \frac{\Delta F^\ddagger(\overline{\delta\ell^2})}{T_F(\overline{\delta\ell^2})} \quad (5.48)$$

for the log ratio of rates. The barrier height is then obtained from eq.s (4.30) and (4.35). It is seen in figure 22 that there is a significant increase in folding rate for structures having larger variance in loop lengths. Structural variance is generated here for a system with parameters in table I, but the loop lengths are given by

$$\ell_i = \bar{\ell} + \alpha (\ell_i^o - \bar{\ell}) \quad (5.49)$$

where ℓ_i^o is taken from the loop length distribution in table I. As α varies from zero to one, the mean loop length $\bar{\ell}$ remains unchanged ($\bar{\ell} \cong 9.14$), but the structural variance $\overline{\delta\ell^2}$ increases (see fig. (22)).

5.I. Tuning energy functions to match desired potentials

We have so far focused on how folding thermodynamics and mechanism are affected by properties of the native structure and distribution of native stability. We can also turn the problem around and seek the native structural properties or stability distribution that would give a specified free energy profile or folding mechanism. To illustrate, fig. 23 shows the free energy potential $F(Q)$ for the 27-mer chain. A fit to the lattice data of ref. [113] for example can be made by annealing the stability distribution $\{\epsilon_i\}$, contact length distribution $\{\ell_i\}$, and/or other parameters with a cost function

$$\text{Cost} = \int_0^1 dQ (F_{\text{target}}(Q) - F(T, \bar{\epsilon}, \{\epsilon_i\}, \bar{\ell}, \{\ell_i\}, s_o, b, \alpha|Q))^2. \quad (5.50)$$

Fits may be made to a fairly arbitrary potential by adjusting the native coupling energies or loop length distribution (the structure), e.g. potentials with and without intermediates, potentials having sharply peaked or flat barriers, etc. See fig. 23B for an example of annealing the energies to fit a target potential with an on-pathway intermediate. Using a sufficiently accurate numerical theory of entropy loss, this method should be able to distinguish between intermediates governed by native structural properties, native energetic stability, or misfolding.

6. SUMMARY AND CONCLUSIONS

In this paper we have introduced refinement and insight into the funnel picture by considering heterogeneity in the folding of well-designed proteins. We have explored in minimally frustrated sequences how folding is effected by heterogeneity in native contact energies, as well as the entropic heterogeneity inherent in folding to a specific three-dimensional native structure. The general method we utilized here should be amenable to systematic refinement, and should be sufficiently accurate to compare with experimental results.

Specifically we found that heterogeneity, whether energetic or entropic in origin, will always lower the folding free energy barrier; see sections 2.2.A, 3.3.B, and 5.5.A, equations (2.12), (3.5), (3.16), (5.18), (5.23),

and (5.39), and figures 11, 12, and 17. This was shown using arguments from the random energy model (section 3.3.B.3.B.1), transition state theory (section 3.3.B.3.B.2), the optimum fluctuation method (section 3.3.B.3.B.3), thermodynamic perturbation theory (section 3.3.B.3.B.4), and free energy functional theory (sections 2.2.A and 5.5.A). For sufficiently well-designed proteins the corresponding rate also increases; see equations (3.6), (3.11), and (5.19), section 5.5.F, and figures 18, 19, and 22. The effects of heterogeneity on barriers and rates are stronger than the effects on transition temperature; see the discussion in the introduction on eq. (1.1), and equation (5.42), and figures 12 and 19. We investigated the effects on the folding barrier due to correlations between energetics and topology, see sections 3.3.A, and 5.5.A, and eq.s (3.3), (5.13) and (5.23), and found that for well-designed proteins the rate may be increased by making initially likely contacts stronger while making unlikely contacts weaker. Thus overall stability is conserved, but the energetic distribution is coupled to the native structure.

For the ensemble of well-designed sequences having a given overall stability, homogeneously ordering sequences have the largest folding free energy barrier. For most structures, where topological factors play an important role, this regime is achieved by introducing a large dispersion in the distribution of native contact energies which in practice would be almost impossible to achieve, see figs 12 and 16C. As we reduce the dispersion in the contact energy distribution and the energies approach a uniform value $\bar{\epsilon}$, the dispersion of contact participations increases and thus the number of folding routes decreases, the free energy barrier decreases and the total configurational entropy increases to a maximum, see sections 3.3.C and 5.5.C.5.C.2. Again, folding temperature is only mildly effected; the prefactor appearing in the rate is probably only mildly effected also, since it is largely a function of T_F/T_G and polymer properties [113]. If many-body forces are not too large the barrier may be reduced to zero, either by adding random native heterogeneity as in section 3.3.B.3.B.4 or by correlating native energy to native structure so that more probable contacts are stronger, as in section 5. The funnel picture, with different structural details, is valid for the above wide range of native contact energy distributions. However, tuning the energies further so that probable contacts have even lower energy (or allowing native energies to have a very large variance) eventually induces the system to take a single or very few folding routes at the transition temperature. A large dispersion of energies is required to achieve this, and in this regime the folding temperature drops well below the glass temperature range, where folding rates are extremely slow.

In section 4.4.B we derived approximate expressions for the conformational entropy functional for a well-designed protein, see eq.s (4.11), (4.26), and (4.27). In section 4.4.B.4.B.1 and Appendix B we generalized the entropy of native core placement (the mixing entropy) used previously in models of folding [96, 97] to account for the effects of chain connectivity; for a highly constrained chain, many contact patterns are degenerate to essentially the same conformation. In section 4.4.B.4.B.2 we derived a general condition for the conformational entropy to be a state function, viz. eq. (4.15). A Hartree approximation was taken to account for the entropy loss of loop closure in the presence of other contacts already formed. This agrees well with the average behavior on the lattice (see fig. 16), however there are important fluctuations away from the mean, indicating many-body correlation effects are present which the theory doesn't account for. Equation (4.26) gives the conformational entropy loss given a distribution of native contact lengths $\{\ell_i\}$. When each $\ell_i \rightarrow \bar{\ell}$, the expression reduces to eq. (4.27) which is the entropy loss for a finite system with mean return length $\bar{\ell}$ for all contacts. When $\bar{\ell} \rightarrow \infty$, (4.27) further reduces to eq. (4.29) which is the entropy loss for a polymer system in the Flory mean-field theory [100].

Residues in proximity are assumed to be in contact energetically; the reduction in conformational entropy at low Q to the elimination of conformations which happen to have residues in proximity [96] is not included here because it is a smaller effect than the other contributions to the entropy.

Several experiments support results from our theory. Enhancement of folding rates by weighting entropically likely contacts, as found in sections 3.3.A and 5.5.B, has been observed in *Escherichia coli* Che Y [119]. Depending on the variance of native interactions and how native interaction strength correlates with the entropic likelihood of contact formation, sequences may be designed to fold both faster or slower to the same structure as a wild-type sequence. Enhancements or suppressions of folding rate to a given structure due to changes in sequence are modeled in our theory through changes in native interactions, which induce significant changes in the rate-governing free energy landscape of a well-designed protein. A minimally frustrated sequence may fold to a given native structure by a variety of folding mechanisms (see fig.s 11 and 14), including through both on and off-pathway intermediates (see fig. 23). Thus for example folding in Im7 and Im9 may likely initiate from different places within the native structure depending on the distribution of stability [16]. Folding in the IgG binding domain of protein L may tend to initiate from a specific region of higher stability, indiscernible from the apparently symmetric native structure [120]; contact formation probability at the transition state depends on both energy and entropy, as expressed in equation (4.35). However, for a large range of native energy distributions, barrier heights, and corresponding rates, a funnel folding mechanism is preserved, in

that there are many routes to the native structure, see fig.s 7 and 13. Folding rates in mutant proteins that exceed those of the wild type have been receiving much interest in recent experiments [17, 119, 121–123]; here we saw how these effects can be understood by applying general principles of the energy landscape. Folding rates in the theory were seen to increase with the variance in contact formation probability, a thermodynamic quantity closely related to the dispersion in experimental ϕ values (see fig. 17). The general trend of reduced rate with larger contact order [30] is well captured by the theory (see fig. 20). Additionally, for fixed contact order, folding rate was shown to increase with larger variance in the contact lengths which constitute the native structure (see fig. 22).

Fluctuations in rate due to the effect of sequence perturbations on weakening or strengthening specific non-native kinetic traps or generally changing non-native interaction strength is an interesting topic of future research.

It is important to note that the enhancements or reductions in rate we have explored are mild compared to the enhancement by minimal frustration (funneling the landscape): the fine tuning of rates may be a phenomenon manifested by *in vitro* or *in machina* evolution, rather than *in vivo* evolution. Nevertheless folding heterogeneity may become an important factor for larger proteins, where e.g. stabilizing partially native intermediates may increase the overall rate or prevent aggregation. Adjusting the backbone rigidity or the non-additivity of interactions [61, 85] can also modify the barrier height, possibly as much as the effects we are considering here. There may also be functional reasons for non-uniform folding - malleability or rigidity requirements of the active site may inhibit or enhance its tendency to order.

The notion expounded here that rates increase with heterogeneity at little expense to native stability contrasts with the view that non-uniform folding in real proteins exists merely as a residual signature of incomplete evolution to a uniformly folding protein. Moreover, the phenomenon that fluctuations in native contact energies contribute extensively to the free energy landscape indicates that the prediction of numerical values for folding rates and mechanisms from approximate energy functions may be even more difficult than originally suspected, i.e. even if systematic error in the calculation of potentials is eliminated, $\mathcal{O}(\mathcal{N})$ corrections may still remain.

The amount of route narrowness in folding was introduced as a thermodynamic measure through the mean square fluctuations in a local order parameter. The route measure may be useful in quantifying the natural kinetic accessibility of various structures. While structural heterogeneity is essentially always present, the flexibility inherent in the number of letters of the sequence code limits the amount of native energetic heterogeneity possible. However some sequence flexibility is in fact required for funnel topographies [124] and so is probably present at least to a limited degree.

We have seen here how a very general theoretical framework can be introduced to explain and understand the effects of heterogeneity in native stability and structural topology on such quantities as folding rates, transition temperatures, and the degree of routing in the funnel folding mechanism. Such a theory should be a useful guide in interpreting and predicting future experimental results on many fast-folding proteins.

6.A. Acknowledgments

We thank Peter Wolynes, Hugh Nymeyer, and Cecilia Clementi for their generous and insightful discussions. This work was supported by NSF Bio-Informatics fellowship DBI9974199 and NSF Grant MCB0084797.

A. APPENDIX A

Consider the free energy of eq. (4.8) as the integral over a semi-local free energy density $F(\{Q_i\}) = \sum_i f_i(Q_i, Q) = \sum_i f_i(Q_i, \sum_j Q_j)$. Taking the differential of a new thermodynamic function $G = F + \mu \sum_i Q_i$,

$$\delta G = \sum_i \left[\left(\frac{\partial f_i}{\partial Q_i} \right)_\mu + \mu \right] \delta Q_i + \left[\sum_j Q_j \right] d\mu \quad (\text{A.1})$$

and demanding that $\partial G / \partial Q_j = 0$ for all j Legendre transforms to a new variable μ , with $\partial G / \partial \mu = MQ$. This is equivalent to minimizing the free energy subject to the constraint of fixed Q . The equation $\partial G / \partial Q_j = 0$ means that

$$\frac{\partial f_i}{\partial Q_i} = -\mu \quad (\text{A.2})$$

for all i , which enforces equation (4.35) for each Q_i . The Lagrange multiplier μ is interpreted as the force corresponding to the potential $F(Q)$:

$$\mu = -\frac{1}{M} \frac{\partial F(\{Q_i\})}{\partial Q} \quad (\text{A.3})$$

by the following arguments. From eq. (A.1) $(\partial G/\partial Q_i)_\mu = 0$ is equivalent to $\partial F/\partial Q_i + \mu = 0$ or

$$\mu = -\frac{\partial F}{\partial Q_i} \quad \text{for any } i \quad (\text{A.4})$$

therefore $\mu = -(\partial Q/\partial Q_i)(\partial F/\partial Q) = -(1/M)(\partial F/\partial Q)$. Since the changes w.r.t. to the local order parameter of all the local free energy terms are the same number μ (eq. A.2), this number equals the change in the sum (F) w.r.t. the change in the sum of the Q_i (MQ) (eq. A.3).

Another way to see eq. (A.3) directly is to consider $\partial/\partial(MQ) = \partial/\partial(\sum_{i=1}^M Q_i)$ as the directional derivative $D_{\mathbf{u}}F$ of F in an M -dimensional space along the direction $\nabla Q = \sum_i \hat{i}$ with \hat{i} a unit vector along the i th axis, defined by the i th contact. So

$$\begin{aligned} \frac{\partial F}{\partial \left(\sum_{i=1}^M Q_i\right)} &= \frac{1}{|\nabla Q|} D_{\mathbf{u}}F = \frac{1}{\sqrt{M}} \frac{\nabla Q}{|\nabla Q|} \cdot \nabla F(\{Q_i\}) \\ &= \frac{1}{M} \left(\sum_i \hat{i} \right) \cdot \sum_j \frac{\partial F}{\partial Q_j} \hat{j} = -\frac{\mu}{M} \sum_{ij} \hat{i} \cdot \hat{j} = -\mu. \end{aligned} \quad (\text{A.5})$$

For the two-state potentials considered here μ has two roots which give the positions of the barrier peak and equilibrium unfolded state (where the local force is zero, see inset of fig. (23)).

B. APPENDIX B

In this appendix we compare a simple microscopic model of route entropy $\mathcal{S}_{\text{ROUTE}}(\{Q_i\})$ with the semi-empirical model introduced in section 4.4.B.4.B.1. In the absence of the constraints due to chain connectivity the route entropy is given by eq.s (4.9) and (4.10). Each native contact pattern $\{Q_i\}$ can be expressed on a native contact map, (see e.g. ref. [125]). The idea here is that since several contact patterns correspond to the same constrained state because of chain-connectivity, the contact-map can be coarse-grained into cells inside of which one or more contacts fully constrains the cell. We make a mean-field approximation and group configurations into cells all of the same Q -dependent size, $\omega_Q > 1$, with $\omega_0 = 1$. To clarify, imagine a system with 6 possible native contacts, and 2 made. Eq. (4.9) gives 15 possible native cores, but if $\omega_{1/3} = 2$ there are $3!/1!(3-1)! + 3!/2!(3-2)! = 6$ configurations; the first 3 configurations correspond to 2 contacts together in any one of the 3 renormalized cells, and the second 3 correspond to one contact in two separate cells.

In general if there are MQ contacts made of M total, with a renormalization factor ω_Q , there are

$$\Omega_{\text{ROUTE}}(Q) = \sum_{j=0}^{j_{\text{MAX}}} \frac{(M/\omega_Q)!}{[\text{int}(MQ/\omega_Q + j + 1/2)]! [M/\omega_Q - \text{int}(MQ/\omega_Q + j + 1/2)]!} \quad (\text{B.1})$$

total configurations. Here $j_{\text{MAX}} = \text{int}[\min(MQ, M/\omega_Q) - (MQ/\omega_Q + 1/2)]$. For example if $M = 8$, $MQ = 5$, and $\omega_{5/8} = 2$, there are 5 total configurations instead of 56 assuming binary mixing. In the thermodynamic limit the entropy is obtained from the largest term in the sum of (B.1):

$$\Omega_{\text{ROUTE}}(Q) = \max_{0 \leq j \leq j_{\text{MAX}}} \frac{(M/\omega_Q)!}{[\text{int}(MQ/\omega_Q + j + 1/2)]! [M/\omega_Q - \text{int}(MQ/\omega_Q + j + 1/2)]!}, \quad (\text{B.2})$$

so that taking $\partial \ln \Omega / \partial j = 0$ gives

$$j^*(Q) \cong \frac{M}{\omega_Q} (1/2 - Q) \quad (\text{B.3})$$

$$\text{where } 0 \leq j^*(Q) \leq \min(MQ, M/\omega_Q) - MQ/\omega_Q. \quad (\text{B.4})$$

Letting $\mathcal{J}^*(Q) = Mj^*(Q)$ and applying the boundary condition eq. (B.4) gives

$$\mathcal{J}^*(Q) = \begin{cases} 0 & Q > 1/2 \\ (1/2 - Q)/\omega_Q & 1/2 \geq Q > Q^* \\ Q(1 - 1/\omega_Q) & Q^* \geq Q \geq 0 \end{cases} \quad (\text{B.5})$$

where Q^* solves $Q^* = 1/2\omega_{Q^*}$. The route entropy is then

$$\begin{aligned} \frac{\mathcal{S}_{\text{ROUTE}}(Q)}{M} &= \frac{1}{M} \ln \Omega_{\text{ROUTE}}(Q, \mathcal{J}^*(Q)) \\ &= -\frac{1}{\omega_Q} \ln \omega_Q - \left(\frac{Q}{\omega_Q} + \mathcal{J}^*(Q) \right) \ln \left(\frac{Q}{\omega_Q} + \mathcal{J}^*(Q) \right) \\ &\quad - \left(\frac{1}{\omega_Q} - \frac{Q}{\omega_Q} - \mathcal{J}^*(Q) \right) \ln \left(\frac{1}{\omega_Q} - \frac{Q}{\omega_Q} - \mathcal{J}^*(Q) \right). \end{aligned} \quad (\text{B.6})$$

In the limit of the cell size $\omega_Q \rightarrow 1$, $\mathcal{J}^*(Q) \rightarrow 0$ and eq. (B.6) reduces to the binary fluid mixing entropy eq.s (4.9) and (4.10), but for $\omega_Q > 1$ the mixing entropy is reduced. The dashed line in figure 7 shows a best fit to the lattice data for ω_Q of the form $\exp(\alpha Q^\beta)$. This gives $\alpha \cong 2.08$ and $\beta \cong 1.85$, whose cell size ω_Q is shown in fig. 24.

TABLE I. PARAMETERS USED IN THE ANALYTIC MODEL TO COMPARE WITH SIMULATION

Chain length	Average bonds per residue	Average (homopolymer) attraction per contact	Average extra native stability per contact	Configurational entropy per residue	R.M.S. energy per non-native contact (roughness)	Reduction parameter in route entropy
(N)	(z)	(\bar{E}/zN)	$(\bar{\epsilon})$	(s_o)	(b)	(α)
27	28/27	-0.0	-3.0	1.352	0.0	0.9
loop length distribution		{3, 3, 3, 3, 3, 5, 5, 5, 5, 7, 7, 7, 7, 7, 9, 9, 9, 9, 9, 11, 11, 13, 21, 23, 23, 23}				
energies inducing uniform folding		- {4.9, 4.5, 2.1, 2.6, 2.7, 5.0, 4.1, 2.3, 6.0, 1.0, 2.1, 1.6, 2.5, 4.0, 1.7, 3.0, 5.0, 3.7, 2.0, 2.4, 1.1, 2.1, 3.3, 3.1, 1.0, 5.5, 2.9, 2.0}				

2.A. Figure Captions

FIG. 1 Schematic, lattice, and off-lattice representations of the native structure, characterized through the distribution of contact energies $\{\epsilon_i\}$ and contact entropies $\{s_i\}$, (defined through the distribution of loop lengths $\{\ell_i\}$). The probability to form contact i having energy ϵ_i and loop length ℓ_i is Q_i .

FIG. 2 The fraction of time a contact is made vs. Q , $Q_i^*(Q)$ for folding to the lattice structure shown in fig. 1. Dashed black curves are the result of the functional theory of section 4, using an energy function given by eq. (5.24) with $\alpha = 0.5$. Thin solid curves are Monte Carlo simulation results for folding to this structure, using eq. (5.24) with $\alpha = 1$. Some contacts are formed relatively early while others remain unformed until the protein is largely native; the magnitude of this dispersion in contact formation is captured fairly well by the theory.

FIG. 3 Making contact 1 stronger in the α -spectrin SH3 domain should speed folding more than making contact 2 stronger by the same amount, since contact 1 in the distal loop is more likely to be formed in the transition state than contact 2 in the RT loop. [126, 127].

FIG. 4 The reduction in effective thermodynamic barrier due to the presence of native heterogeneity. The probability of a nucleation event dies off exponentially with barrier height $k \sim \exp(-F/T)$, and the probability distribution $P(F)$ of barrier heights is centered on \bar{F}^\ddagger and has some width in the presence of energetic and entropic inhomogeneity. The effective nucleation rate $k(F) \sim P(F)k(F)$ has a maximum at an effective barrier $F^*(T) < \bar{F}^\ddagger$ corresponding to the optimum fluctuation. Figure adapted from ref. [78].

FIG. 5 Free energy vs. fraction of native contacts Q , obtained from off-lattice simulations using a uniform G \bar{o} potential to the native structure of CheY (data from [39]). Fluctuations in the free energy profile here depend solely on how the native topology affects the entropy at partial degrees of nativeness. The profile observed is the optimal fluctuation from uniform ordering, given the native structure under study.

FIG. 6 Illustration of partially native configurations consisting of native cores and the surrounding polymer halo. The core may be globular or ramified.

FIG. 7 Route entropy for the 27-mer with native structure shown in fig. 1. The dotted curve is the putative binary fluid mixing entropy in the absence of the backbone. The solid curves includes a prefactor $(1 - Q^\alpha)$ corresponding to the entropic asymmetry of applying contacts to an unconstrained polymer and removing contacts from a fully constrained polymer, described in the text. The data are for the 27-mer lattice model shown in fig. 1 [128], and are obtained for low Q values by making subsets of $M(1 - Q)$ contacts repulsive, MQ contacts attractive, and then finding the most native-like state in a low temperature quench. For high Q values they are obtained by making random sets of $M(1 - Q)$ contacts repulsive, and counting the remaining native cores which are distinct. This method finds the reduction in binary fluid mixing entropy due to chain connectivity and particular native topology of the protein under study. We assume that α is essentially constant for a given native structure, independent of the distribution of native energies. The computation treats all contact formation probabilities on an equal footing (all $Q_i = Q$), and so the route entropy plotted is an upper limit to the actual route entropy present. See also fig. 13. Using eq.s (4.11), (4.12) with $Q_i = Q$ gives $\alpha = 1.37$ for the best fit to the lattice structure in fig. 1, while somewhat smaller values of α fit the free energy function best (table I). The dashed curve is the best fit of a simple microscopic theory to the route entropy, described in Appendix B.

FIG. 8 Illustrating constraints on the functional form of the entropy, given it must be a state function. Path (1) dashed, Path (2) solid.

FIG. 9 The total energy of the 27-mer lattice model, in units of $\bar{\epsilon}$, as a function of the fraction of native contacts Q , for native energies $\{\epsilon_i^*\}$ tuned to give a homogeneous transition state (thin solid curve), for uniform native energies $\{\bar{\epsilon}\}$ (thick solid line), for native energies $\{\epsilon_i^o\}$ which induce enough heterogeneity to eliminate the barrier (long dashed), and for native energies $\{\epsilon_i^R\}$ which induce a folding mechanism by only a few routes (short dashed).

FIG. 10 Total entropy vs. Q for the 27-mer lattice model. The maximal solid curve is for $\{\epsilon_i\} = \{\bar{\epsilon}\}$. For these energies the entropy has its highest value. The entropy for the homogeneous funnel with tuned energies $\{\epsilon_i^*\}$ (thin solid curve) is significantly lower. For native energies $\{\epsilon_i^o\}$ which eliminate the barrier (long dashed), the entropy is essentially unchanged, since changes in entropy near the extremum (where $\{\epsilon_i\} = \{\bar{\epsilon}\}$) are second order. The entropy for a route-like folding mechanism (short dashed) is lower than the other curves since the route entropy (eq. 4.11) no longer contributes significantly to the total entropy at temperatures where the native state is stable.

FIG. 11 Free energy vs. Q in units of $\bar{\epsilon}$ at the folding temperature $T_F(\{\epsilon_i\})$ for the 27-mer lattice model (TOP) and theory (BOTTOM), for the energy functions described in the text and previous 2 figures.

FIG. 12 Barrier height in units of native interaction strength as a function of RMS native energetic variance in the same units, for simulations of the G \bar{o} lattice model. The barrier height is multi-valued here because of energetic correlations with loop lengths, as described in the text. Also shown is the folding transition temperature, which remains fairly constant until the barrier disappears and the RMS energetic variance becomes large. Another measure of how well-designed the protein is weights T_F by the root entropy per monomer at the barrier peak, which also remains fairly constant until the barrier disappears (thin solid line with squares).

FIG. 13 Route entropy for the 27-mer lattice model (Top) and free energy functional theory (Bottom), as given by equation (4.11). The route entropy is a thermodynamic measure of how labile or itinerant the native core of the protein is at intermediate stages of folding. Different line styles represent different folding mechanisms described in the text (the same code is used as in fig.s 9, 10, and 11).

FIG. 14 Contact formation probability $Q_i(Q)$ as a function of Q . (TOP) Simulation results, (BOTTOM) Analytical theory. (LEFT) Coupling energies are tuned to induce a route-like folding mechanism, (RIGHT) coupling energies are tuned to induce a uniform funnel folding mechanism through the barrier peak.

FIG. 15 Flory entropy of the system, defined by subtracting the route entropy from the total entropy, as a function of the fraction of native contacts. The top plot is the result from simulating the lattice 27-mer. The bottom plot is the result of the analytical theory (the same line styles as fig.s 9, 10, 11, and 13 are used).

FIG. 16 Comparison of the theory and simulations, for a set of energies inducing an intermediate folding barrier height in (A),(B) ($\alpha_{\text{SIM}} = 1.0$, $\alpha_{\text{THRY}} = 0.5$ in eq. (5.24)), and for energies ϵ_i^* which induce a uniform folding mechanism (C). (A) Contact probabilities at the barrier peak. (B) Contact probability vs. log loop length. Crosses are the lattice data, squares are their average, and the solid line is the theory result (eq. 4.35 with eq.s (4.19) and (4.20)). (C) plots the energy fluctuation required to tune the system to fold uniformly vs. the entropy fluctuation each loop has. The solid line is the theoretical result eq. (5.13) and the data points with error bars are extracted from the simulations.

FIG. 17 Free energy barrier at the transition temperature T_F in units of $\bar{\epsilon}$, vs. the route measure at the barrier peak $\mathcal{R}(Q^\ddagger)$. (Solid line) theoretical result for a model with parameters in table I. (Long dashed) idealized funnel with $\ell_i = \bar{\ell}$, and $\epsilon_i = \bar{\epsilon}$ initially. (Short dashed) perturbation result from eq. (5.39).

FIG. 18 Simulating a long Monte Carlo run for the 27-mer lattice model at T_F yields an exponential distribution of first passage times to the folded state from the unfolded state (inset B, plotted for the point with $\mathcal{R} = 0.11$), indicating a single time-scale governs the kinetics. The mean of the distribution (the folding time τ_F) is plotted here for a few energy functions which result in varying amounts of routing through the barrier by eq. (5.37). For comparison, the folding time determined from $\tau = \text{const.} \times \exp(-\Delta F^\ddagger/T_F)$ is shown as a solid line, with $\Delta F^\ddagger(\mathcal{R})$ taken from the lattice data in fig. 17 (there are error bars about the points defining this line which are not shown). The folding time is a decreasing function of the route measure $\mathcal{R}(Q^\ddagger)$. (Inset A) The log of the folding time varies nearly linearly with the barrier height indicating that the prefactor is roughly constant while the native energy distributions are varied.

FIG. 19 The relative barrier height decreases more strongly than the relative folding temperature, as a function of route measure at the barrier peak (eq. 5.37). Thus the condition for the folding rate to increase, eq. (5.42), is satisfied.

FIG. 20 Dependence of the free energy profile $F(Q)$ at T_F on the mean loop length $\bar{\ell}$, for the analytic model with length $N = 50$, $\ell_i = \bar{\ell}$, and $\epsilon_i = \bar{\epsilon}$ (eq.s (4.30) and (4.31)). $\bar{\ell}$ labels each curve. The barrier undergoes an increase that is stronger initially. The inset plots the barrier height as a function of $\bar{\ell}$, in units of $\bar{\epsilon}$. The trend in barrier height with $\bar{\ell}$ shown here is a lower limit to the full theoretical dependence given in eq. (5.44).

FIG. 21 Entropy vs. Q for $\epsilon_i = \bar{\epsilon}$ and $\ell_i = \bar{\ell}$, for various $\bar{\ell}$. The contact order $\equiv \bar{\ell}/N$ ($N = 27$ here) labels each curve. Results are for the theory with parameters in table I (c.f eq. 4.27). As $\bar{\ell}$ increases, more entropy is lost initially, leading to a larger free energy barrier and correspondingly slower folding rate. (INSET): The model shows a weak increasing dependence of θ'_m value with contact order, defined here as the relative degree of partial order at the barrier peak: $\theta'_m \equiv (Q^\ddagger - Q_U)/(1 - Q_U)$. The trends seen here are again lower limits to the full dependence on $\bar{\ell}$ given in eq. (5.44), we illustrate just the mean-field term here.

FIG. 22 Log of the ratio of rates given by eq. (5.48) as a function of structural variance $\overline{\delta\ell^2}$ at fixed $\bar{\ell}$, obtained by following the recipe of eq. (5.49). (Dashed) Approximate perturbation result of eq. (5.47). (Solid) Full non-perturbative result using eq.s (4.30) and (4.35), which accounts for changes in the unfolded free energy with increasing variance. The barrier is calculated at T_F , which changes only mildly with $\overline{\delta\ell^2}$ until the barrier height approaches zero at $\overline{\delta\ell^2}/\bar{\ell}^2 \approx 0.25$.

FIG. 23 (A) Squares are the free energy potential obtained in ref. [113] to the structure shown in fig. 1B. Solid curve is a fit to the data by annealing the native coupling energies using eq. (5.50). (INSET):

The effective force $\mu(Q)$. The two zeros of μ occur at the positions of the unfolded state Q^o and barrier peak Q^\ddagger . **(B)** Fitting to a potential containing an on-pathway intermediate by adjusting the coupling energies $\{\epsilon_i\}$. The illustration here is for a system of length $N = 57$ with 142 contacts, having the native loop length distribution of the α -spectrin SH3 domain [39]. The unfolded and folded states are at $Q = 0, 1$ since the bulk limit ($\bar{\ell}Q \gg 1$) was taken in determining the potentials here (c.f. eq. 4.29). A specific part of the protein is biased energetically with successively larger strength to achieve an on-pathway intermediate. This could also have been achieved in the theory by adjusting the native structure to have contacts which are relatively likely entropically. Finding the set(s) of loop lengths $\{\ell_i^*\}$ that best fit a given target potential is relevant to the problem of which native structures would typically have such a potential, if native energetic features are not as important. Progression of the effective force $\mu(Q)$ is also shown in **(C)**; $\mu(Q)$ corresponding to the potential with the intermediate has 3 roots, one at the intermediate position, one at the barrier peak, and one at a smaller barrier peak near the unfolded state. **(D)** The barrier height here deviates from its typical dependence on the route-measure, since the route-measure becomes largest at the value of order parameter characterized by the intermediate, rather than at the barrier peak.

FIG. 24 Renormalized mixing cell size ω_Q as a function of Q , assuming the form $\omega_Q = \exp(\alpha Q^\beta)$ with $\alpha = 2.08$ and $\beta = 1.85$, which are the numbers giving the best fit to the lattice data (dashed curve in fig. 7).

2.B. Figures

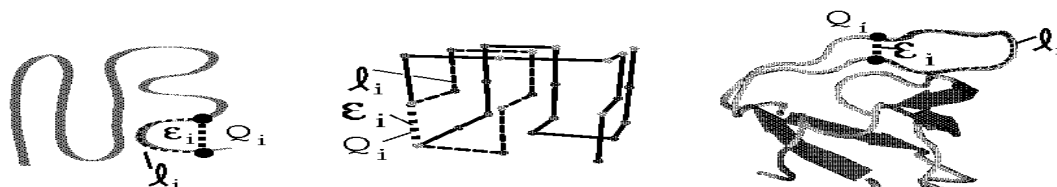


FIG. 1.

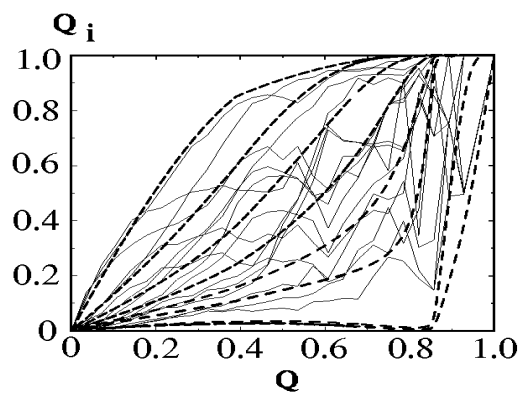


FIG. 2.

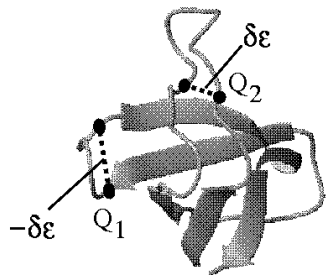


FIG. 3.

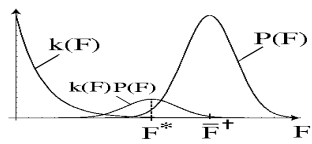


FIG. 4.

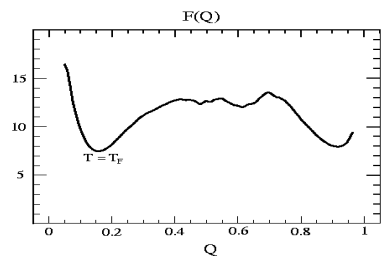


FIG. 5.

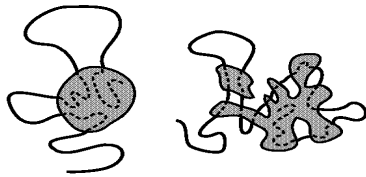


FIG. 6.

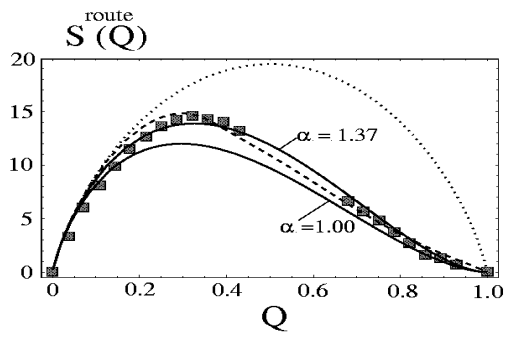


FIG. 7.

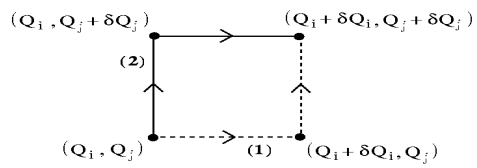


FIG. 8.

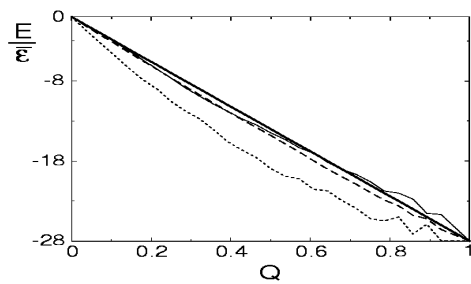


FIG. 9.

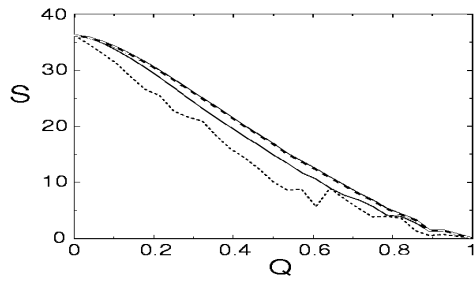


FIG. 10.

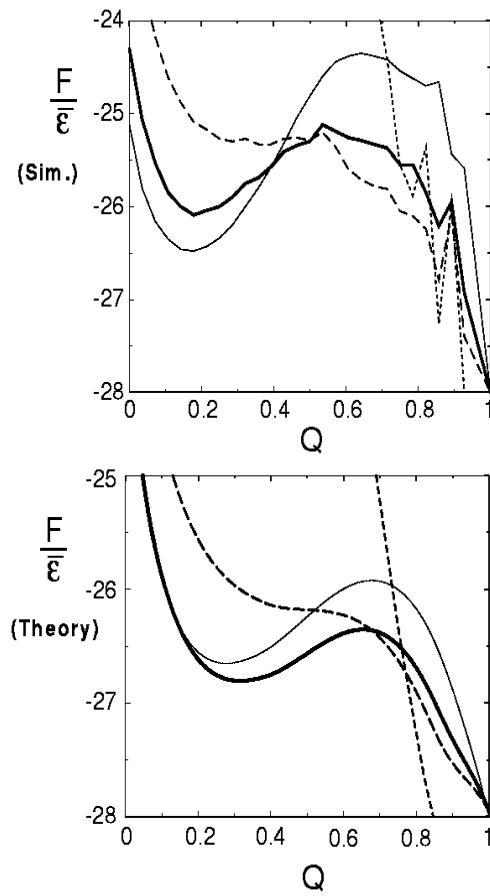


FIG. 11.

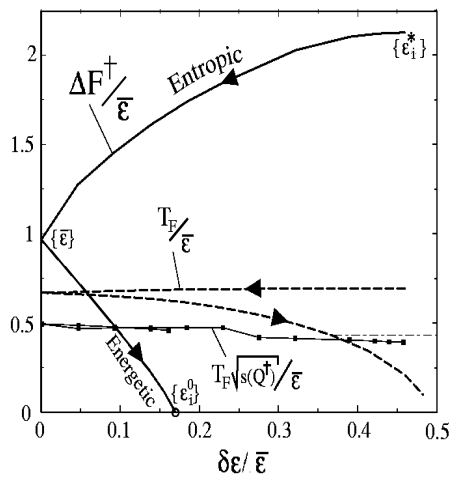


FIG. 12.

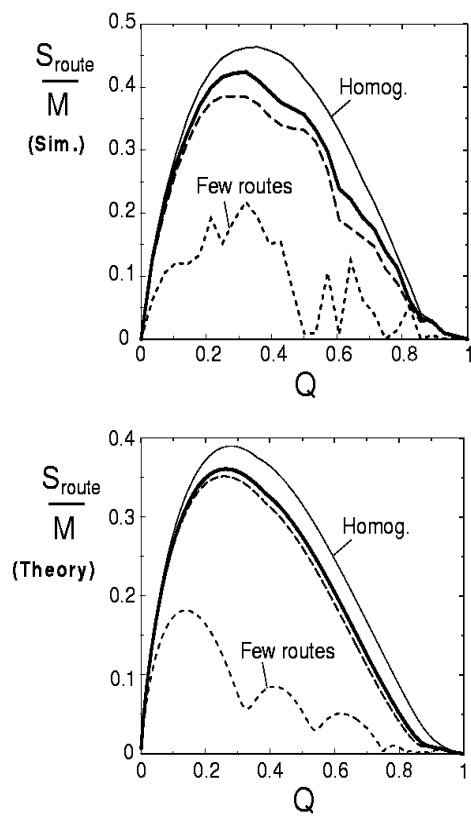


FIG. 13.

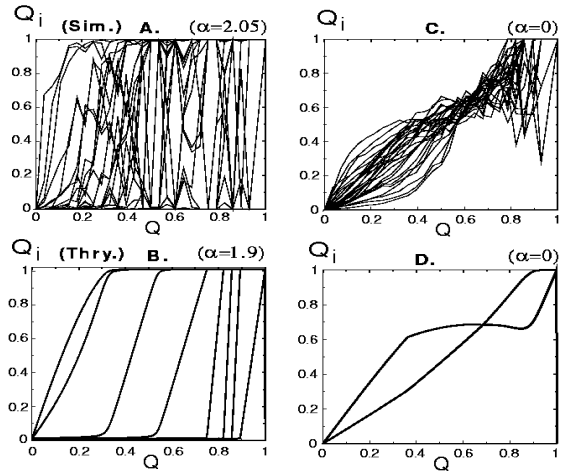


FIG. 14.

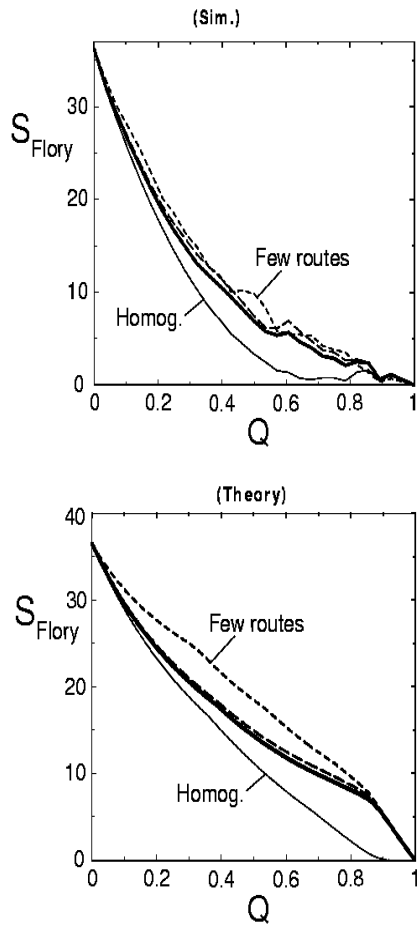


FIG. 15.

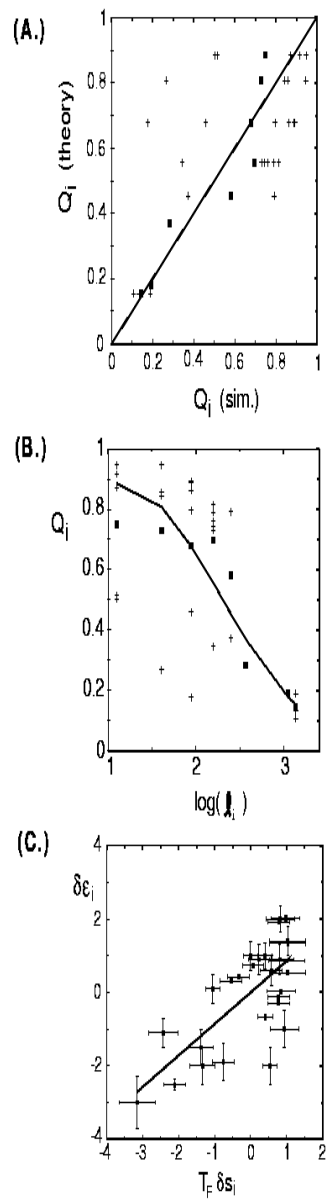


FIG. 16.

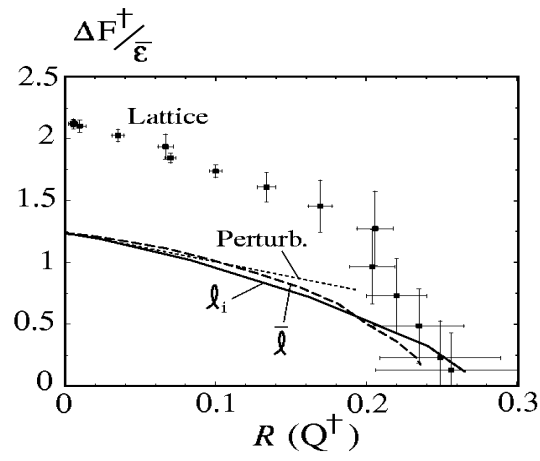


FIG. 17.

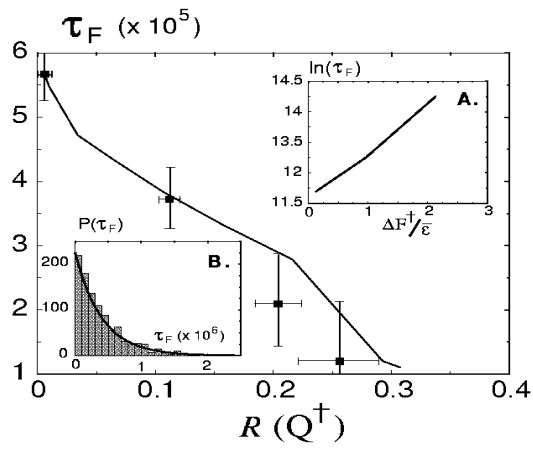


FIG. 18.

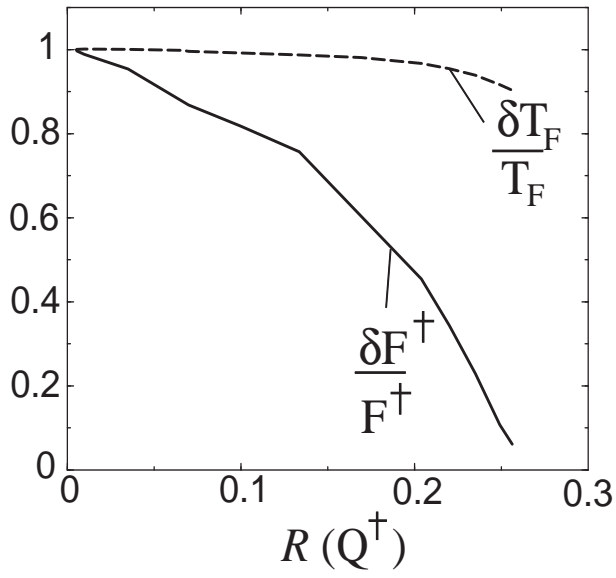


FIG. 19.

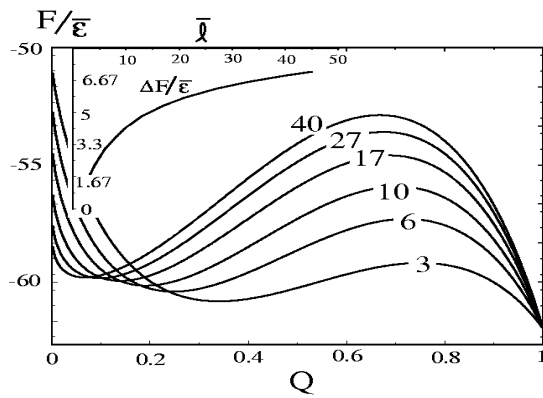


FIG. 20.

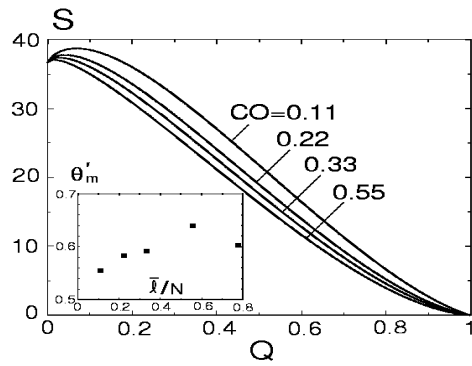


FIG. 21.

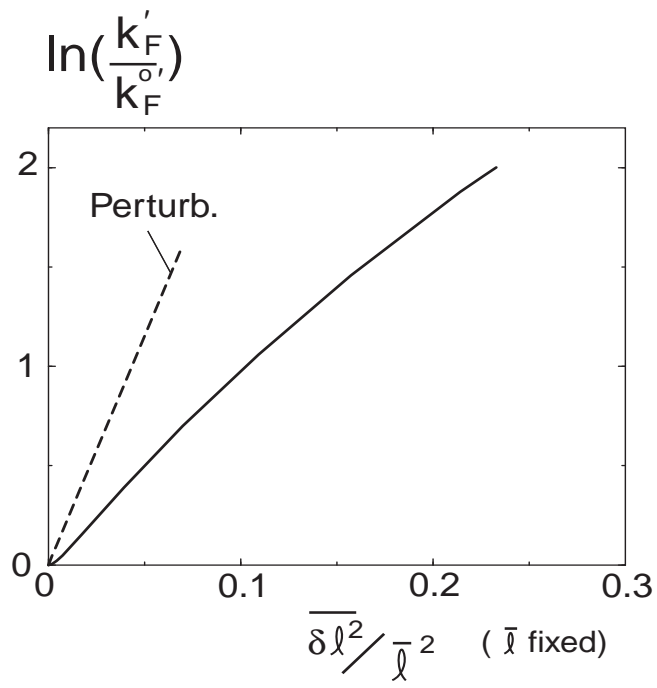


FIG. 22.

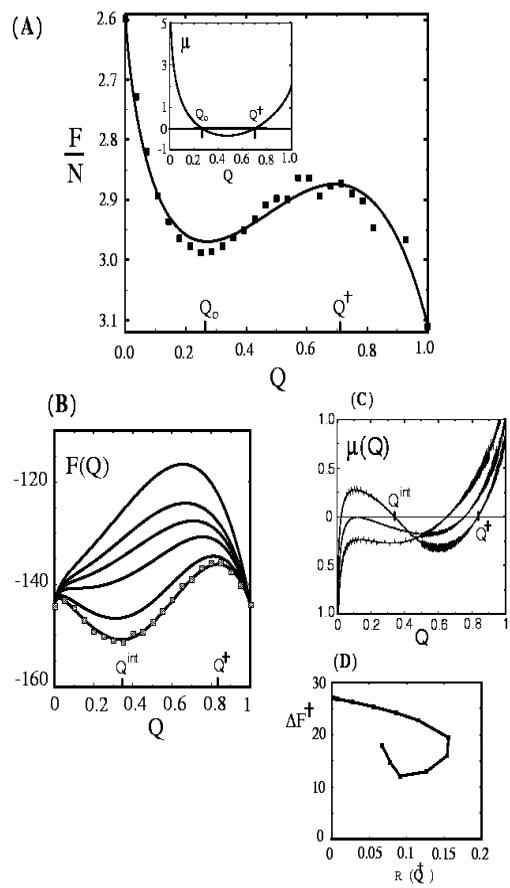


FIG. 23.

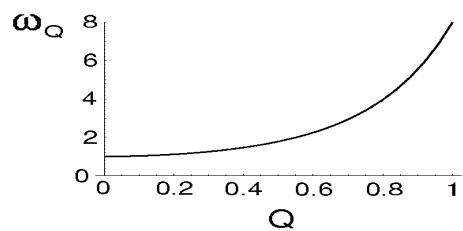


FIG. 24.

-
- [1] P. G. Wolynes, in *Spin Glasses and Biology*, edited by D. L. Stein (World Scientific, Singapore, 1992), pp. 225–259.
- [2] J. D. Bryngelson, J. N. Onuchic, N. D. Socci, and P. G. Wolynes, *Proteins* **21**, 167 (1995).
- [3] K. A. Dill *et al.*, *Protein Sci* **4**, 561 (1995).
- [4] K. D. Ball *et al.*, *Science* **271**, 963 (1996).
- [5] K. A. Dill and H. S. Chan, *Nat. Struct. Biol.* **4**, 10 (1997).
- [6] T. Veitshans, D. Klimov, and D. Thirumalai, *Folding and Design* **2**, 1 (1997).
- [7] J. N. Onuchic, Z. Luthey-Schulten, and P. G. Wolynes, *Annu Rev Phys Chem* **48**, 545 (1997).
- [8] V. S. Pande, A. Y. Grosberg, and T. Tanaka, *Biophys J* **73**, 3192 (1997).
- [9] C. M. Dobson, A. Sali, and M. Karplus, *Angew Chem Int Ed Engl* **37**, 868 (1998).
- [10] T. Garel, H. Orland, and E. Pitard, in *Spin Glasses and random fields*, edited by A. P. Young (World Scientific, River Edge, N.J., 1998).
- [11] C. L. Brooks, M. Gruebele, J. N. Onuchic, and P. G. Wolynes, *Proc Nat Acad Sci USA* **95**, 11037 (1998).
- [12] A. R. Fersht, *Structure and mechanism in protein science*, 1st ed. (W. H. Freeman and Co., New York, 1999).
- [13] M. Gruebele, *Annu Rev Phys Chem* **50**, 485 (1999).
- [14] D. J. Wales and H. A. Scheraga, *Science* **285**, 1368 (1999).
- [15] J. N. Onuchic *et al.*, *Adv. Protein Chem.* **53**, 87 (2000).
- [16] N. Ferguson *et al.*, *J Mol Biol* **286**, 1597 (1999).
- [17] D. E. Kim, H. Gu, and D. Baker, *Proc Nat Acad Sci USA* **95**, 4982 (1998).
- [18] P. M. Dalessio and I. J. Ropson, *Biochemistry* **39**, 860 (2000).
- [19] V. I. Abkevich, A. M. Gutin, and E. I. Shakhnovich, *Biochemistry* **33**, 10026 (1994).
- [20] J. N. Onuchic, N. D. Socci, Z. Luthey-Schulten, and P. G. Wolynes, *Folding and Design* **1**, 441 (1996).
- [21] D. K. Klimov and D. Thirumalai, *J Mol Biol* **282**, 471 (1998).
- [22] L. Li, L. A. Mirny, and E. I. Shakhnovich, *Nature Struct Biol* **7**, 336 (2000).
- [23] R. A. Goldstein, Z. A. Luthey-Schulten, and P. G. Wolynes, *Proc Nat Acad Sci USA* **89**, 4918 (1992).
- [24] J. D. Bryngelson and P. G. Wolynes, *Proc Nat Acad Sci USA* **84**, 7524 (1987).
- [25] P. E. Leopold, M. Montal, and J. N. Onuchic, *Proc Nat Acad Sci USA* **89**, 8721 (1992).
- [26] E. I. Shakhnovich and A. M. Gutin, *Proc Nat Acad Sci USA* **90**, 7195 (1993).
- [27] J. N. Onuchic, P. G. Wolynes, Z. Luthey-Schulten, and N. D. Socci, *Proc Nat Acad Sci USA* **92**, 3626 (1995).
- [28] E. Bornberg-Bauer and H. S. Chan, *Proc Nat Acad Sci USA* **96**, 10689 (1999).
- [29] N. E. G. Buchler and R. A. Goldstein, *J Chem Phys* **111**, 6599 (1999).
- [30] K. W. Plaxco, K. T. Simons, and D. Baker, *J Mol Biol* **277**, 985 (1998).
- [31] V. Munoz and W. A. Eaton, *Proc Nat Acad Sci USA* **96**, 11311 (1999).
- [32] A. R. Fersht, *Proc Nat Acad Sci USA* **97**, 1525 (2000).
- [33] E. Alm and D. Baker, *Proc Nat Acad Sci USA* **96**, 11305 (1999).
- [34] B. A. Shoemaker, J. Wang, and P. G. Wolynes, *J Mol Biol* **287**, 675 (1999).
- [35] O. V. Galzitskaya and A. V. Finkelstein, *Proc Nat Acad Sci USA* **96**, 11299 (1999).
- [36] J. E. Shea, J. N. Onuchic, and C. L. Brooks, *Proc Nat Acad Sci USA* **96**, 12512 (1999).
- [37] D. S. Riddle *et al.*, *Nat. Struct. Biol.* **11**, 1016 (1999).
- [38] R. Du *et al.*, *J Chem Phys* **111**, 10375 (1999).
- [39] C. Clementi, H. Nymeyer, and J. N. Onuchic, *J Mol Biol* **298**, 937 (2000).
- [40] C. Clementi, P. A. Jennings, and J. N. Onuchic, *Proc Nat Acad Sci USA* **97**, 5871 (2000).
- [41] D. M. Taverna and R. A. Goldstein, *Biopolymers* **53**, 1 (2000).
- [42] A. Maritan, C. Micheletti, A. Trovato, and J. R. Banavar, *Nature* **406**, 287 (2000).
- [43] S. S. Plotkin and J. N. Onuchic, *Proc Nat Acad Sci USA* **97**, 6509 (2000).
- [44] B. A. Shoemaker, J. Wang, and P. G. Wolynes, *Proc. Nat. Acad. Sci. USA* **94**, 777 (1997).
- [45] B. A. Shoemaker and P. G. Wolynes, *J Mol Biol* **287**, 657 (1999).
- [46] A. M. Gutin, V. I. Abkevich, and E. I. Shakhnovich, *Proc Nat Acad Sci USA* **92**, 1282 (1995).
- [47] S. A. Radford, C. M. Dobson, and P. A. Evans, *Nature* **358**, 302 (1992).
- [48] Y. Bai, T. R. Sosnick, L. Mayne, and S. W. Englander, *Science* **269**, 192 (1995).
- [49] E. M. Boczko and C. L. Brooks, *Science* **269**, 393 (1995).
- [50] T. Lazaridis and M. Karplus, *Science* **278**, 1928 (1997).
- [51] F. B. Sheinerman and C. L. Brooks, *Proc Nat Acad Sci USA* **95**, 1562 (1998).
- [52] A. R. Fersht, A. Matouschek, and L. Serrano, *J Mol Biol* **224**, 771 (1992).
- [53] A. Horovitz and A. Fersht, *J Mol Biol* **224**, 733 (1992).
- [54] M.-H. Hao and H. Scheraga, *Physica A* **244**, 124 (1997).

- [55] J. M. Sorenson and T. Head-Gordon, *Folding and Design* **3**, 523 (1998).
- [56] D. K. Klimov and D. Thirumalai, *Folding and Design* **3**, 127 (1998).
- [57] K. Lum, D. Chandler, and J. D. Weeks, *J Phys Chem* **103**, 4570 (1999).
- [58] S. Takada, Z. Luthey-Schulten, and P. G. Wolynes, *J Chem Phys* **110**, 11616 (1999).
- [59] R. B. Prince, J. G. Saven, P. G. Wolynes, and J. S. Moore, *J Am Chem Soc* **121**, 3114 (1999).
- [60] A. Kolinski, W. Galazka, and J. Skolnick, *Proteins: Struct. Funct. and Genetics* **26**, 271 (1996).
- [61] S. S. Plotkin, J. Wang, and P. G. Wolynes, *J Chem Phys* **106**, 2932 (1997).
- [62] M. P. Eastwood and P. G. Wolynes, preprint (unpublished).
- [63] The native backbone topology is more precisely specified by a vector parameterized by the arc-length along the polymer chain, $\mathbf{r}(s)$, but it is difficult to apply the formalism starting from this description.
- [64] J. F. Douglas and T. Ishinabe, *Phys Rev E* **51**, 1791 (1995).
- [65] J. D. Bryngelson and P. G. Wolynes, *J Phys Chem* **93**, 6902 (1989).
- [66] J. J. Portman, S. Takada, and P. G. Wolynes, *Phys Rev Lett* **81**, 5237 (1998).
- [67] R. Du *et al.*, *J Chem Phys* **108**, 334 (1998).
- [68] J. K. Percus, in *The liquid state of matter: Fluids, simple and complex*, edited by E. Montroll and J. Lebowitz (North-Holland, Amsterdam, 1982).
- [69] R. Evans, in *Fundamentals of inhomogeneous fluids*, edited by D. Henderson (Dekker, New York, 1992).
- [70] J. D. Gunton, M. S. Miguel, and P. S. Sahni, in *Phase Transitions and Critical Phenomena*, edited by C. Domb and J. L. Lebowitz (Academic Press, New York, 1983), Vol. 8, pp. 267–466.
- [71] H. G. Bohr and P. G. Wolynes, *Phys Rev A* **46**, 5242 (1992).
- [72] We will generally set Boltzmann’s constant $k_B = 1$ in this paper, so temperatures have units of energy, and entropies are in units of k_B .
- [73] Later in the paper we will assume all quantities are thermally equilibrated, and the averages will indicate sums over native contacts, e.g. $Q = \langle Q_i \rangle$. The meaning should be clear from the context.
- [74] In this section only M is the total magnetization.
- [75] We thank H. Nymeyer for helpful discussions on this argument.
- [76] B. Derrida, *Phys Rev B* **24**, 2613 (1981).
- [77] V. G. Karpov, *Phys Rev B* **50**, 9124 (1994).
- [78] V. G. Karpov and D. W. Oxtoby, *Phys Rev B* **54**, 9734 (1996).
- [79] I. M. Lifshitz, *Adv. Phys* **13**, 483 (1964).
- [80] B. I. Halperin and M. Lax, *Phys. Rev.* **148**, 722 (1966).
- [81] J. Zittartz and J. S. Langer, *Phys. Rev.* **148**, 741 (1966).
- [82] L. D. Landau and E. M. Lifshitz, *Statistical Physics*, 3 ed. (Pergamon Press, Oxford, 1980).
- [83] Averaging over native disorder in calculating $\overline{Q_i}$ leaves the residual dependence on loop entropy for each contact probability, which is then summed using $\sum_i \overline{Q_i} = MQ$.
- [84] P. G. Wolynes, *Proc Nat Acad Sci USA* **94**, 6170 (1997).
- [85] A. Kolinski, A. Godzik, and J. Skolnick, *J Chem Phys* **98**, 7420 (1993).
- [86] M. Vendruscolo, R. Najmanovich, and E. Domany, *Phys Rev Lett* **82**, 656 (1999).
- [87] R. Becker and W. Doring, *Ann. Phys. (Leipzig)* **24**, 719 (1935).
- [88] J. Lothe and G. M. Pound, *J Chem Phys* **36**, 2080 (1962).
- [89] H. Reiss, J. L. Katz, and E. R. Cohen, *J Chem Phys* **48**, 5553 (1967).
- [90] J. Lothe and G. M. Pound, in *Nucleation*, edited by A. C. Zettlemoyer (Dekker, New York, 1969), p. 109.
- [91] J. S. Langer, *Ann. Phys. (N.Y.)* **41**, 108 (1967).
- [92] M. E. Fisher, *Physics* **3**, 255 (1967).
- [93] C. Unger and W. Klein, *Phys Rev B* **29**, 2698 (1984).
- [94] J. W. Cahn and J. E. Hilliard, *J Chem Phys* **28**, 258 (1958).
- [95] J. S. Langer, *Ann. Phys. (N.Y.)* **54**, 258 (1969).
- [96] S. S. Plotkin, J. Wang, and P. G. Wolynes, *Phys Rev E* **53**, 6271 (1996).
- [97] V. S. Pande, A. Y. Grosberg, and T. Tanaka, *Folding and Design* **2**, 109 (1997).
- [98] A. Fernández, K. S. Kostov, and R. S. Berry, *J Chem Phys* **112**, 5223 (2000).
- [99] This term contains in principle a resummation of all the moments of a virial expansion of the entropy $S_v(\{Q_i^f\}|\{Q_i^o\}) = \sum_i s_i^o \times (Q_i^f - Q_i^o) + \sum_{i,j} s_{i,j}^o \times (Q_i^f - Q_i^o) \times (Q_j^f - Q_j^o) + \dots$ which is a slowly convergent expansion consisting of 2-body, 4-body and higher order terms.
- [100] P. J. Flory, *J Am Chem Soc* **78**, 5222 (1956).
- [101] A. Gutin and E. Shakhnovich, *J Chem Phys* **100**, 5290 (1994).
- [102] A. V. Finkelstein and A. Y. Badretdinov, *Molecular Biology* **31**, 391 (1997).
- [103] H. S. Chan and K. A. Dill, *J Chem Phys* **92**, 3118 (1990).
- [104] K. A. Dill, K. M. Fiebig, and H. S. Chan, *Proc Nat Acad Sci USA* **90**, 1942 (1993).
- [105] M.-H. Hao and H. A. Scheraga, *J. Phys. Chem.* **98**, 4940 (1994).
- [106] We could equivalently have explicitly invoked this by introducing the Lagrange constraint $\sum_i Q_i = MQ$ into the

problem from the outset.

- [107] L. S. Itzhaki, D. E. Otzen, and A. R. Fersht, *J Mol Biol* **254**, 260 (1995).
- [108] H. Nymeyer, N. D. Socci, and J. N. Onuchic, *Proc Nat Acad Sci USA* **97**, 634 (2000).
- [109] Note that by the structure of eq. (4.20), eq (5.13) is satisfied for all Q , i.e. when the energies are tuned to extremize ΔF^\ddagger , the Q_i are all equal essentially for all Q . Thus in the model there is full symmetry in the ordering of the protein. However, when the entropy is exactly counted, and also when the entropy cutoff mentioned after eq. (4.29) is present, $Q_i(Q) = Q$ only at the barrier peak. See fig. 14C and 14D.
- [110] A. Sali, E. Shakhnovich, and M. Karplus, *Nature* **369**, 248 (1994).
- [111] N. D. Socci and J. N. Onuchic, *J Chem Phys* **103**, 4732 (1995).
- [112] V. I. Abkevich, A. M. Gutin, and E. I. Shakhnovich, *J Mol Biol* **252**, 460 (1995).
- [113] N. D. Socci, J. N. Onuchic, and P. G. Wolynes, *J Chem Phys* **104**, 5860 (1996).
- [114] S. S. Plotkin, submitted to *Proteins: Struct. Funct. and Genetics* (unpublished).
- [115] F. T. Wall and P. J. Flory, *J Chem Phys* **19**, 1435 (1951).
- [116] R. T. Deam and S. F. Edwards, *Phil. Trans. R. Soc. A* **280**, 317 (1976).
- [117] J. Wang, S. S. Plotkin, and P. G. Wolynes, *J. Phys. I France* **7**, 395 (1997).
- [118] S. Takada, J. J. Portman, and P. G. Wolynes, *Proc Nat Acad Sci USA* **94**, 23188 (1997).
- [119] A. R. Viguera, V. Villegas, F. X. Aviles, and L. Serrano, *Folding and Design* **2**, 23 (1996).
- [120] D. E. Kim, C. Fisher, and D. Baker, *J Mol Biol* **298**, 971 (2000).
- [121] V. Munoz and L. Serrano, *Folding and Design* **1**, R71 (1996).
- [122] S. J. Hagen, J. A. Hofrichter, A. Szabo, and W. A. Eaton, *Proc Nat Acad Sci USA* **93**, 11615 (1996).
- [123] B. M. Brown and R. T. Sauer, *Proc Nat Acad Sci USA* **96**, 1983 (1999).
- [124] P. G. Wolynes, *Nature Struct Biol* **4**, 871 (1997).
- [125] K. M. Fiebig and K. A. Dill, *J Chem Phys* **98**, 3475 (1992).
- [126] J. C. Martinez, M. T. Pisabarro, and L. Serrano, *Nature Struct Biol* **5**, 721 (1998).
- [127] V. P. Grantcharova, J. V. Santiago, D. Baker, and D. S. Riddle, *Nature Struct Biol* **5**, 714 (1998).
- [128] We are grateful to H. Nymeyer for providing the lattice data for this plot.